ORIGINAL PAPER

Accessory mineral U–Th–Pb ages and ^{40}Ar/^{39}Ar eruption chronology, and their bearing on rhyolitic magma evolution in the Pleistocene Coso volcanic field, California

Justin I. Simon · Jorge A. Vazquez · Paul R. Renne · Axel K. Schmitt · Charles R. Bacon · Mary R. Reid

Abstract We determined Ar/Ar eruption ages of eight extrusions from the Pleistocene Coso volcanic field, a long-lived series of small volume rhyolitic domes in eastern California. Combined with ion-microprobe dating of crystal ages of zircon and allanite from these lavas and from granophyre geothermal well cuttings, we were able to track the range of magma-production rates over the past 650 ka at Coso. In ≤230 ka rhyolites we find no evidence of protracted magma residence or recycled zircon (or allanite) from Pleistocene predecessors. A significant subset of zircon in the ∼85 ka rhyolites yielded ages between ∼100 and 200 Ma, requiring that generation of at least some rhyolites involves material from Mesozoic basement. Similar zircon xenocrysts are found in an ∼200 ka granophyre. The new age constraints imply that magma evolution at Coso can occur rapidly as demonstrated by

significant changes in rhyolite composition over short time intervals (≤10's to 100's ka). In conjunction with radio-isotopic age constraints from other young silicic volcanic fields, dating of Coso rhyolites highlights the fact that at least some (and often the more voluminous) rhyolites are produced relatively rapidly, but that many small-volume rhyolites likely represent separation from long-lived mushy magma bodies.

Communicated by T.L. Grove.

J. I. Simon (✉) · P. R. Renne
University of California, Berkeley & Berkeley Geochronology Center, Berkeley, CA, USA
e-mail: simon@eps.berkeley.edu

J. A. Vazquez
California State University, Northridge, Northridge, CA, USA

A. K. Schmitt
University of California, Los Angeles, Los Angeles, CA, USA

C. R. Bacon
United States Geological Survey, Menlo Park, CA, USA

M. R. Reid
Northern Arizona University, Flagstaff, AZ, USA

Introduction

An increasing number of studies find that long "crystal residence times" are typical of silicic domes (see review by Reid 2003). In contrast, it appears that large volume eruptions contain datable crystal populations that are more homogeneous and on average closer in age to eruption (Simon et al. 2008). The reason for this is unclear, but may be due to the greater energy input required to produce large eruptions. Further studies bearing on the inverse correlation between crystal (i.e., "magma") residence time with erupted volume, and moreover on criteria for the possible cause, appear warranted. The spectrum of bimodal continental volcanism ranges from systems that are composed of small monogenetic basaltic centers and rare, small-volume rhyolites (e.g., Coso) to voluminous, dominantly silicic caldera systems (e.g., Long Valley). The existence of numerous small-volume rhyolite domes of the Coso volcanic field located in eastern California in the absence of a voluminous caldera-related eruption presents the opportunity to study the evolution of an end-member among long-lived silicic

magma centers and to improve our understanding of the time scales of silicic magma processes. Further dating of Coso rhyolites provides an opportunity to explore and refine ideas on how large shallow silicic magma systems develop and how quickly their magmatic and eruptive behavior evolves (e.g., Bacon et al. 1981).

In this paper we report $^{40}Ar/^{39}Ar$ sanidine ages and U–Th–Pb accessory mineral ages for late Pleistocene Coso rhyolite lavas. The $^{40}Ar/^{39}Ar$ data yield more precise eruption ages than the K–Ar ages previously reported for Coso rhyolites and other volcanic rocks by Duffield et al. (1980). Several extrusions at Coso are nearly aphyric and contain little to no feldspar. In such cases we apply similar $^{40}Ar/^{39}Ar$ methods to potassium-rich obsidian samples, which along with feldspar ages, provide an improved eruption chronology. Crystallization and melt differentiation occur at magmatic temperatures at times that may significantly predate eruption (cf. Simon et al. 2008; and references therein). In favorable cases a comparison between isotopic dating of accessory minerals and the age of individual eruptions can be used to constrain the time scales over which physiochemical variations in magmas are produced (e.g., Vazquez and Reid 2002). At Coso the age distribution, chemistry, and textures of zircons from the ∼0.6 Ma Devils Kitchen rhyolite led Miller and Wooden (2004) to suggest that the erupted magma was remobilized intrusions and/or near-solidus crystal mush that were emplaced in the crust over an ∼200 ka period.

There is little evidence for cognate crystal recycling or protracted magma residence time when $^{40}Ar/^{39}Ar$ eruption ages are compared to zircon and allanite crystallization ages in the younger (≤230 ka) Coso rhyolites. Moreover, during this time period we find clear evidence for crustal assimilation and crystal inheritance as indicated by Mesozoic zircon ages. The absence of protracted residence times and of evidence for recycling in the younger (≤230 ka) Coso rhyolites contrast sharply with the discrete, i.e., 10's to 100's ka age spans reported to represent pre-eruption crystal residence ("magma residence times" *senso lato*) in the older ∼0.6 Ma Devils Kitchen rhyolite, as well as at other large silicic magma centers, e.g., the Whakamaru Tuff at Taupo Volcano, New Zealand (Brown and Fletcher 1999), some post-caldera and the caldera-related rhyolites at Yellowstone (Bindeman, et al. 2001; Vazquez and Reid 2002), and a number of Long Valley rhyolites (Reid and Coath 2000; Simon and Reid 2005; Simon, et al. 2007). These differences amplify our need to distinguish between evidence for protracted fractional crystallization differentiation within long-lived shallow magma reservoirs and evidence for remobilization of crystals formed in relatively short-lived melt bodies (cf. Bachmann and Bergantz 2003; Bacon and Lowenstern 2005; Charlier et al. 2005; Schmitt and Simon 2004) and ultimately why there exists such a

range of behavior within and among long-lived silicic magma centers.
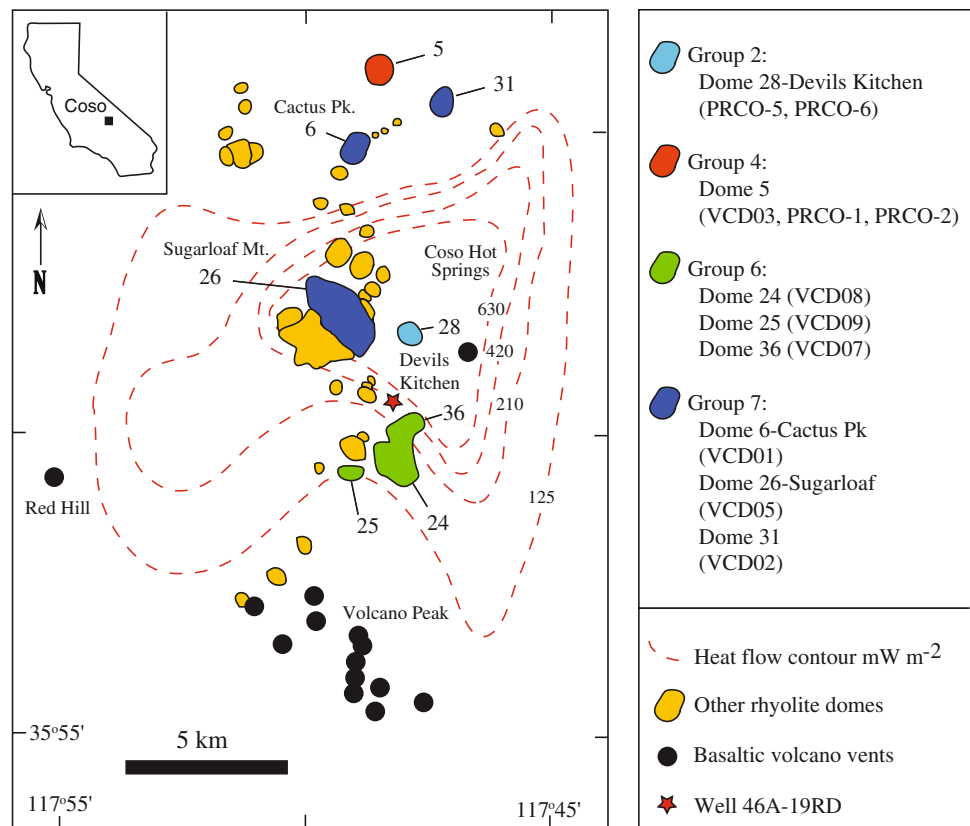
Geology of Coso volcanic field

The Coso volcanic field of California is located at the margin of the Basin and Range province, east of the Sierra Nevada and Owens Valley (Fig. 1). The Coso field is underlain by pre-Cenozoic granitic plutons, dioritic to gabbroic plutons, and metamorphic basement rocks (Duffield et al. 1980). Collectively these units compose the Coso Range that is structurally separated from the main body of the composite Sierra Nevada batholith along the Sierra Nevada fault zone. Although a single K–Ar biotite age of ∼90 Ma has been reported, most of the granitic plutons in the Coso Range are inferred to be Late Mesozoic, whereas most of the mafic plutons and metamorphic rocks appear to be somewhat older (Duffield et al. 1980). Chen and Moore (1979) report concordant ∼150 Ma U–Pb zircon ages for dikes related to the Independence swarm, trending northwest–southeast in the Alabama Hills (northwest of the Coso Range) and in the Argus Range (east of Coso). There are younger east-west-trending dikes intruding ∼102 Ma granitic plutons locally in the northern part of the Range that contain zircon as young as ∼83 Ma that were probably emplaced during the Late Cretaceous (Kylander-Clark et al. 2005).

Miocene and Pliocene basalt flows that represent the initiation of Late Cenozoic volcanism are now tilted, whereas more recent flows are flat lying indicating that uplift of the Coso Range and the onset of volcanism appear to have been nearly contemporaneous (Duffield et al. 1980). Monastero et al. (2005) report that the Quaternary rhyolite field and active geothermal system are located in a releasing bend of the dextral strike-slip Sierra Nevada fault zone above a nascent metamorphic core complex. Monastero et al. (2005) concluded that magma generation was related to crustal thinning, shallowing of the mid-crust, and proximity to the asthenospheric mantle.

Interest in the Coso geothermal system has prompted multidisciplinary research on the volcanic field since the 1970s (e.g., see *JGR*, volume 85, 1980 special issue), including geologic mapping (Duffield and Bacon 1981) and K–Ar geochronology (Duffield et al. 1980; Lanphere et al. 1975). Bacon et al. (1981) assigned the 38 Quaternary rhyolite extrusions to seven groups, each of which consisted of chemically similar units that had similar apparent eruption ages. Although the precision and accuracy of $^{40}Ar/^{39}Ar$ dating techniques are typically superior to those of dates obtained by the K–Ar method, which may be biased by excess ^{40}Ar contamination (e.g., Renne et al. 1997) or incomplete extraction of argon from sanidine (e.g., McDowell 1983), the K–Ar results are adequate to

Fig. 1 Map showing Pleistocene volcanism at Coso in eastern California (after Bacon 1982). Sampling locations for dated rhyolites and granophyre drill cuttings from geothermal well shown for reference

define the general history of the Coso volcanic field. Volcanism began ~6 Ma. Since ~4 Ma, ~35 km³ of lava has erupted in the Coso Range and about 30 km³ of this was emplaced in the Pliocene between ~4 and 2.5 Ma (Duffield et al. 1980). In this study we have focused on the Pleistocene rhyolites (≤1.1 Ma), ~2 km³ of extruded rhyolite likely related to the active magma and geothermal systems. Heat-flow measurements (Combs 1980) imply that the volume of intruded silicic magma may be as much as 100 times greater (Bacon et al. 1981). Similar to that characteristic of the Pliocene buildup, the volume of silicic eruptions during the Pleistocene increased (since ~0.25 Ma) toward the present (Duffield et al. 1980).

Pleistocene volcanism at Coso is bimodal in composition and is composed of basalt and rhyolite. Basaltic vents tend to lie outside of the focus of silicic magmatism at any given time, an observation often interpreted as evidence that basaltic extrusion is hindered by the existence of a low-density magma body (cf. Bacon 1985). Moreover, frequent seismicity (Walter and Weaver 1980), as well as teleseismic P-delay tomography (Reasenberg et al. 1980) provides evidence for a magma body with a current estimate for the top of the body at ~5 km below the surface (Wilson et al. 2003). Pyroxene thermobarometry of Pliocene (~3.5 to 2 Ma) and Pleistocene (~1.1 to 0.1 Ma) basalts at Coso suggests that crystallization occurred at

~15 km (~550 MPa) and then ~25 to 30 km (~900 MPa) depths, respectively (Mordick and Glazner 2006). Manley and Bacon (2000) used the Al-in-hornblende barometer to show that mineral growth within the ~0.6 to 0.3 Ma rhyolites imply that the depth to the top of the silicic magma body was ~10 km (~270 MPa) and that by ~0.04 Ma it had risen to ~5.4 km (140 MPa). Following Bacon et al. (1981), Mordick and Glazner (2006) concluded that Pleistocene basalts likely provided heat needed to generate Pleistocene rhyolite and may have been trapped beneath the Pleistocene rhyolite magma body, a possible explanation for why the Pleistocene basalts records greater depths than the Pliocene basalts.

Whether or not a single long-lived shallow magma chamber was present throughout Pleistocene time, Duffield et al. (1980; and references therein) reported that some level of geothermal actively likely existed during this interval. Duffield et al. (1980) described evidence for fumaroles thought to be related to the ~0.6 Ma Devils Kitchen dome and the adjacent Nicol area, and also noted past hydrothermal activity near Sugarloaf Mountain and Coso Hot Springs based on a K–Ar age of 234 ± 22 ka for an overlying basalt flow that is unaffected by thermal spring activity. More recent evidence of geothermal activity is demonstrated by pollen encapsulated in a travertine deposit at Wheeler Prospect (~2 km south of Coso Hot Springs) that yields an

age of ~ 12 ka (Kovac et al. 2006; and reference therein). Today the abundant fumaroles and rigorously boiling mud holes, high seismicity (Walter and Weaver 1980), high heat flow (~ 120 to $\sim 1,045$ mW/m^2 in the center of the field, which is above present day Basin and Range levels ≤ 110 mW/m^2; Combs 1980), and the generation of >250 MW of electrical power (Monastero 2002) are manifestations of the active geothermal system.

Description of rhyolites and dated materials

At least 38 rhyolite domes and lava flows were extruded at Coso during the Pleistocene. The dome names (numbers), their field relationships, and their major and trace element compositions used here to develop models for the petrogenetic and eruption history of the magma system come from Duffield et al. (1980) and Bacon et al. (1981). In general, Coso rhyolites are crystal-poor with the two oldest domes (38 and 28) and a third dome (5) located at the north end of the field being the exceptions. Typical crystal contents range from ~ 1 to <0.001 wt.% (Bacon et al. 1981). Despite their low crystal contents, Coso rhyolites commonly contain xenocrysts that can be distinguished by composition and morphology. Detailed descriptions of their mineral assemblages (including the presence of multiple populations of ferromagnesian silicate phases) can be found in Manley and Bacon (2000). Representative rhyolites have been selected for this study and for completeness a brief description and their mineral assemblages are included in Table 1. Samples were collected by J. Vazquez (VCD series) and by W. Amidon, K. Farley, and P. Renne (PRCO series) separately under the guidance of F. Monastero. The granophyre cuttings from injection well 46A-19RD obtained during the Coso Enhanced Geothermal Systems Experiment were provided by J. Moore. Allanites from dome 24 come from a sample collected by C. Bacon. The "Devils Kitchen" rhyolite (dome 28) was sampled twice (PRCO-5 and PRCO-6). Miller and Wooden (2004) report that almost all Devils Kitchen zircons are euhedral, but that many have anhedral, embayed cores with euhedral overgrowths. Mafic enclaves and xenocrysts are also present (Bacon and Metz 1984). Three samples from dome 5 were collected (VCD03, PRCO-2, PRCO-3). PRCO-2 and PRCO-3 are from the surface of the dome obtained ~ 100 m apart. Obsidian was obtained from domes 17 (VCD01) and 20 (VCD06), but contain inadequate amounts of feldspar. Likewise, from the sample material collected of dome 25 (VCD09) we obtained insufficient accessory minerals for dating purposes. Rare aphyric mafic enclaves and forsteritic olivine xenocrysts have been reported for both dome 24 and 25 lavas (Bacon and Metz 1984; Manley and Bacon 2000). The allanites from domes 6, 24, and 26 are up to ~ 100 μm in size and are anhedral to subhedral

while zircons are typically subhedral and up to ~ 200 μm in size with inclusions of apatite and glass. Both allanite and zircon are microphenocrysts in the holohyaline groundmass. Injection well 46A-19RD is located ~ 1 km north of dome 24 about a third of the distance to Sugarloaf Mountain (dome 26). The subsurface granophyre was sampled as drill cuttings from a depth interval of 11,420–11,440 ft ($\sim 3,485$ m) in well 46A-19RD (Kovac et al. 2006).

Methods

^{40}Ar/^{39}Ar dating of obsidian and alkali feldspar

Obsidian samples were crushed to produce fragments of brown glass, free of phenocrysts, and cleaned in distilled water with an ultrasonic disintegrator. Feldspars were separated from crystal-poor obsidian, perlitic, and pumiceous glasses. Alkali feldspars were concentrated by heavy liquid and magnetic separation techniques, and cleaned by short ultrasonic baths of dilute hydrofluoric acid followed by distilled water. Alkali feldspars were distinguished from residual plagioclase using immersion oils and petrographic methods, and then selected by hand for analysis. Two irradiations were used. The VCD-series materials, along with 37 Alder Creek feldspars (1,193 ± 1 ka; Nomade et al. 2005), used to monitor the neutron fluence, were irradiated at the Oregon State University TRIGA reactor in the Cd-lined CLICIT facility for 30 min within a series of stacked aluminum disks, permitting precise monitoring of both vertical ($J = \sim 1.341 \times 10^{-4}$ to $\sim 1.350 \times 10^{-4}$) and lateral (negligible) flux gradients. The PRCO-series materials, along with 54 Alder Creek feldspar crystals, were irradiated in a similar fashion in a single aluminum disk [$J = \sim 1.41 (\pm 0.01) \times 10^{-4}$]. Total fusion and step-heating feldspar and glass analyses were performed. Glasses and three to eight grain feldspar aliquots were analyzed by laser step-heating following procedures described previously (Nomade et al. 2005; and references therein). Age spectra derived from laser step-heating of samples from previously dated domes show that excess ^{40}Ar contamination likely biased some K–Ar results. However, ^{40}Ar/^{39}Ar analyses of the studied rhyolites with disturbed model ages (i.e., assuming atmospheric initial Ar), but well-defined Ar isochrons are considered to provide accurate eruption ages (Fig. 2). When comparing U–Th–Pb crystal ages and ^{40}Ar/^{39}Ar eruption ages, it is important to consider the intercalibration bias between the two systems. This bias, mainly a product of error in the electron capture decay constant for ^{40}K (Min et al. 2000), is small (ca. 1%) compared with the differences considered in this paper. For comparison with existing data, a shift upward of ~ 10 ka to the age of the Devils Kitchen rhyolite

Table 1 Mineralogy and sample description of studied Coso rhyolites and granophyre

Sample	Lithology	Crystal content	Mineralogy	Enclaves	Comments
Dome 5					
VCD03	Obsidian	∼2 (wt.%)	Qtz, Sa, Pl, Mag, Bt, and accessory Ap ± Zrn		
PRCO-2	Obsidian				From dome surface
PRCO-3	Obsidian				From dome surface
Dome 6 (Cactus Peak)					
VCD01	Obsidian	∼1 (wt.%)	Qtz, Sa, Pl, Mag, Bt, Fa, and accessory Ap, Aln, and Zrn		
Dome 17					
VCD01	Obsidian	Aphyric			
Dome 20					
VCD06	Obsidian	Aphyric			
Dome 24					
VCD08	Pumiceous vitrophyre	∼0.01 (wt.%)	Qtz, Afs, Pl, Mag, Ilm, Opx, Cpx, Bt, Fo ± Fa, accessory Ap, Aln, and Zrn	Rare aphyric mafic	
Dome 25					
VCD09	Pumiceous vitrophyre	∼0.01 (wt.%)	Qtz, Afs, Pl, Mag, Ilm, Opx, Cpx, Bt, Fo ± Fa, accessory Ap, Aln, and Zrn	Rare aphyric mafic	
Dome 26 (Sugarloaf Mt.)					
VCD05	Obsidian	∼0.01 (wt.%)	Qtz, Sa, Afs, Pl, Mag, Ilm, Opx, Cpx, Hbl, Bt, accessory Zrn and Aln		
Dome 28 (Devils Kitchen)					
PRCO-5	Crystal-rich vitrophyre	∼15 (wt.%)	Qtz, Sa, Pl, Mag, Ilm, Opx, Cpx, Hbl, Bt, Fa, accessory Zrn	Porphyritic mafic	
PRCO-6	Crystal-rich vitrophyre				
Dome 31					
VCD02	Gray obsidian	∼1 (wt.%)	Afs (anorthoclase), Pl, Mag, and accessory Ap, Aln, and Zrn		
Dome 36					
VCD07	Shiny gray vitrophyre	Nearly aphyric			
Injection well 46A-19RD					
Depth of ∼3485 m	Granophyre	Mostly crystalline, w/ some glass	Qtz, Pl, Afs, Bt, accessory Zrn and minor secondary Cal and Chl		From well cuttings

Qtz quartz, *Sa* sanidine, *Afs* alkali-feldspar, *Pl* plagioclase, *Mag* magnetite, *Ilm* ilmenite, *Cpx* clinopyroxene, *Opx* orthopyroxene, *Hbl* hornblende, *Bt* biotite, *Fa* fayalitic olivine, *Fo* forsteritic olivine, *Ap* apatite, *Aln* allanite, *Zrn* zircon, *Cal* calcite, *Chl* chlorite

is needed to corrected for the bias. This is made using the ^{40}K decay constants of Mundil et al. (2006), and the $^{40}Ar/^{39}Ar$ standard basis of Renne et al. (1998).

Ion microprobe U–Th and U–Pb ages of zircon and allanite

Accessory minerals were separated by heavy liquid techniques. U–Th disequilibrium dating was performed on individual zircon and allanite crystals using the UCLA Cameca ims 1270 secondary ion mass spectrometer (ion microprobe), based on techniques from Reid et al. (1997), Schmitt (2006), and Vazquez and Reid (2004). An <20–50 nA mass-filtered $^{16}O^{-}$-beam was focused into a ∼35 μm × 30 μm oval spot. Secondary ions were accelerated at 10 keV with an energy bandpass of 50 eV and analyzed at a mass resolution of <4,800 for zircon and ∼9,000 for allanite using an axial electron multiplier
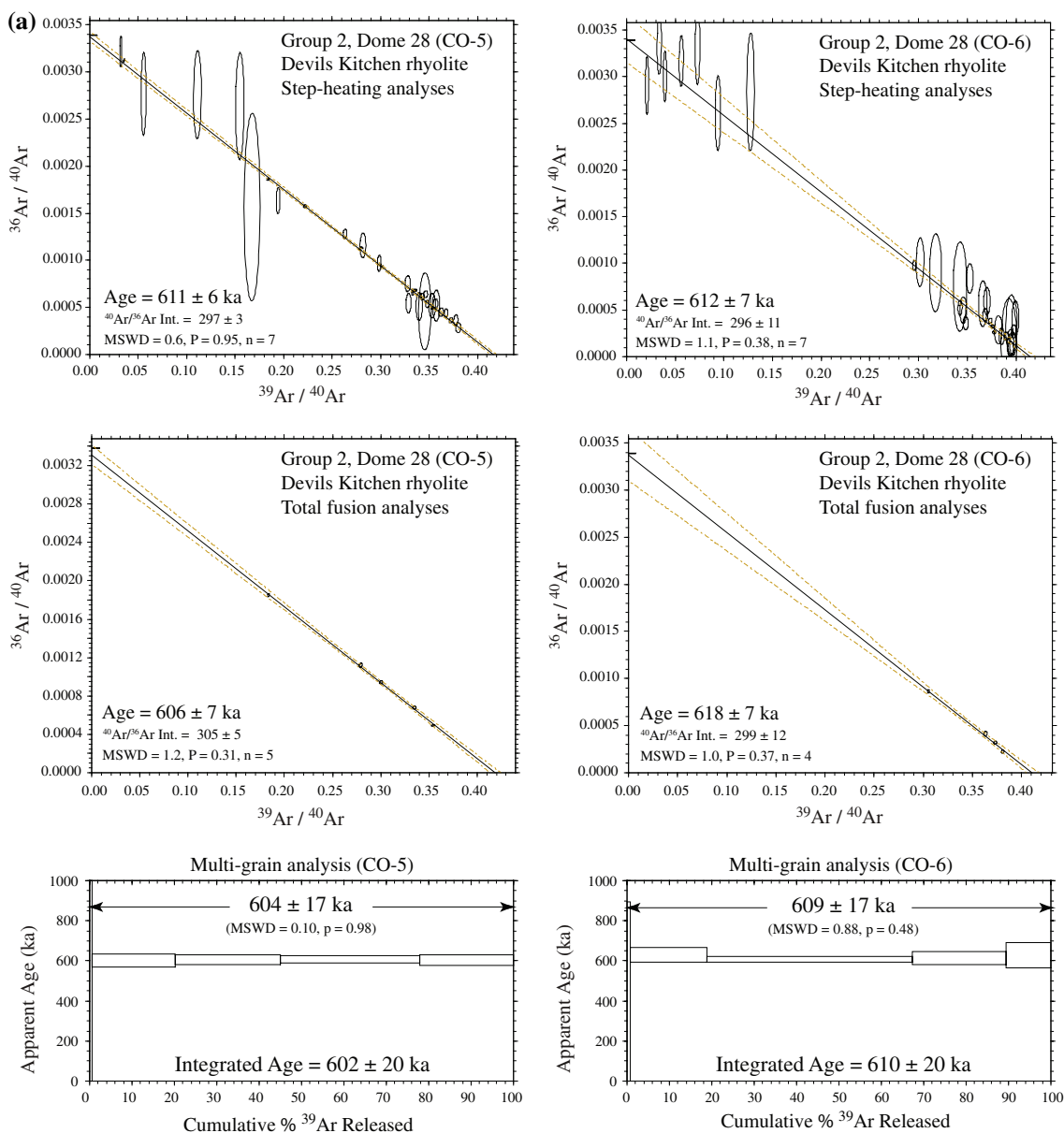
Fig. 2 $^{40}Ar/^{39}Ar$ ages for feldspar and glass of selected high-silica rhyolite domes and lava flows of the Coso volcanic field. Dated domes include eight samples from four of seven chemically distinct Pleistocene rhyolite groups. Analyses are alkali-feldspar except for Sugarloaf Mountain which is obsidian and include: **a** Multi-grain step-heating and total fusion isochron and plateau $^{40}Ar/^{39}Ar$ ages of the Group 2 Devils Kitchen rhyolite (CO-5, CO-6), **b** multi-grain

step-heating and total fusion isochron and plateau $^{40}Ar/^{39}Ar$ ages of the Group 4 dome 5 rhyolite (CO-2, CO-3, and VCD-03), **c** multi-grain step-heating $^{40}Ar/^{39}Ar$ isochron ages for Group 6 rhyolite domes 24 (VCD08), 25 (VCD09), and 36 (VCD07), and **d** multi-grain step-heating isochron and plateau $^{40}Ar/^{39}Ar$ ages for Group 7 Sugarloaf Mountain (VCD05), Cactus Peak (VCD01), and dome 31 rhyolites (VCD02)

collector in peak jumping mode. For zircon, relative sensitivities for ^{238}UO and ^{232}ThO were calibrated by measuring the radiogenic $^{206}Pb/^{208}Pb$ ratio of concordant reference zircons AS-3 and 91,500 (Paces and Miller 1993; Wiedenbeck et al. 1995). Ion microprobe analysis of allanites from the Bishop Tuff (777 ka) and Mesa Falls Tuff (1.2 Ma) yield $^{230}Th/^{238}U$ within error of secular equilibrium, as expected for allanites older than ~500 ka (Reid et al. 1997). Coso zircons found to be in secular

equilibrium were analyzed for their $^{238}U-^{206}Pb$ crystallization ages, employing established methods (e.g., Dalrymple et al. 1999; Quidelleur et al. 1997). When possible and appropriate (i.e., young), individual U–Pb ages were ^{207}Pb-corrected for common Pb using a typical whole rock initial common $^{207}Pb/^{206}Pb$ ratio of 0.818 (this study). The common lead composition is likely to be largely intrinsic, i.e., incorporated at the time of crystallization and trapped within inclusions, but could also be
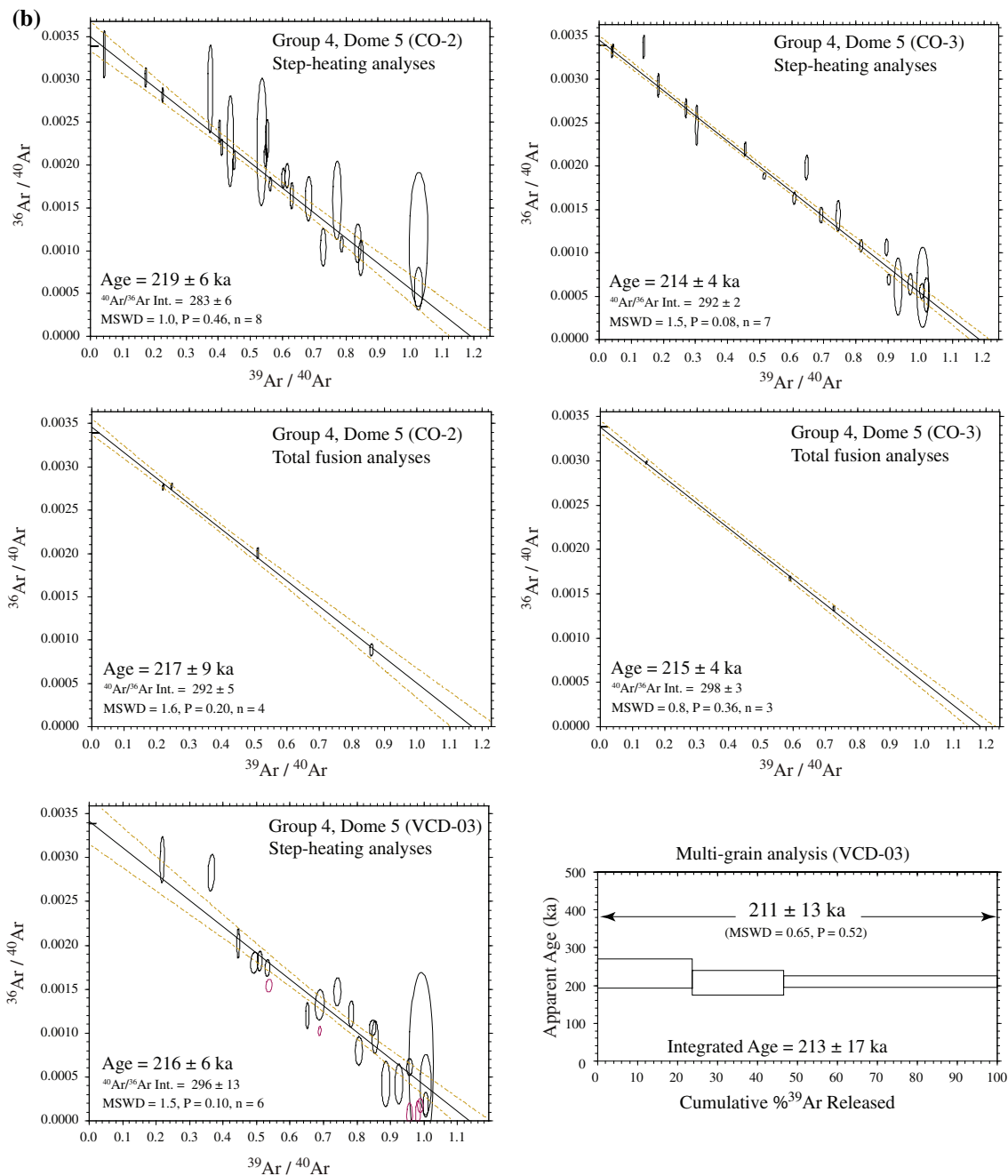
Fig. 2 continued

partly due to contamination by Southern California anthropogenic Pb, which has a similar composition (Sañudo-Wilhelmy and Flegal 1994). The [207]Pb-corrected ages are also adjusted for initial U–Th disequilibrium due to the deficit in radiogenic [206]Pb originating from the initial deficit in [230]Th relative to [238]U following Schärer (1984). The magnitude of this deficit can be estimated by comparing the Th/U ratios in zircon to those of the host magmas (i.e., glass, Table 3). The absolute effect of this correction (typically adding 80–90 ka, e.g., Simon et al.

2008) is accurate to ∼10 ka, allowing for the range of whole rock Th/U ratios observed. Most applications of this correction assume that the melts were in secular equilibrium with respect to [238]U–[230]Th when the zircons crystallized. However, [230]Th excesses during crystallization will lead to calculated ages that overestimate the true ages by 4 ka per 5% [230]Th excess. One of our sampled rhyolites (Dome 24) contains an ∼10% [230]Th excess, whereas the Sugarloaf rhyolite contains an ∼5% [238]U excess. Whole rock samples were analyzed for their U and
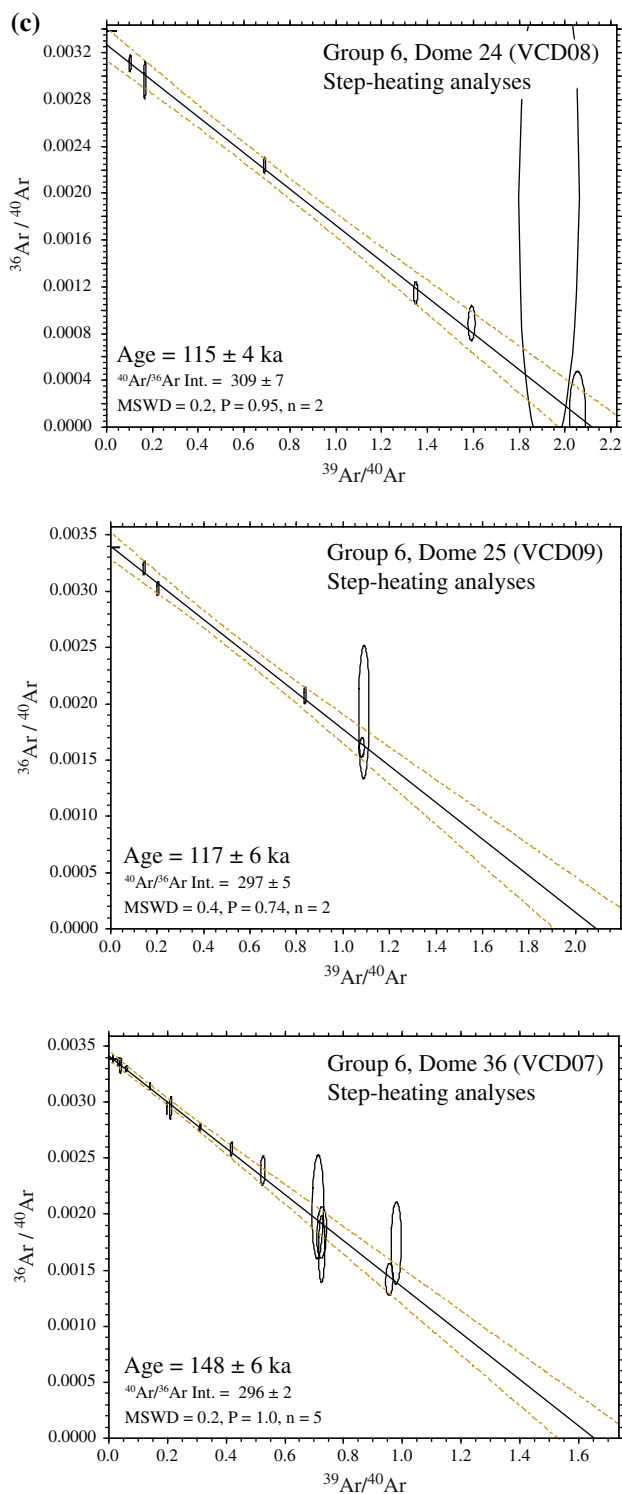
(c)

Fig. 2 continued

Th isotope compositions by thermal ionization mass spectrometry (TIMS) at UCLA following the procedure of Bohrson and Reid (1998). Blanks were negligible (<0.01% for U and Th). Analysis of UCSC-Th-A standard during analyses yielded a weighted mean $^{232}Th/^{230}Th$ of

$170,254 \pm 0.3\%$ ($2\,\sigma$, $n = 3$). The whole rock compositions of the Coso extrusions were assumed to be representative of the magma from which the granophyre zircons grew, and were used to calculate model ^{238}U–^{230}Th crystallization ages.

Ion microprobe zircon Ti abundances

Selected zircons in this study were analyzed for Ti abundances subsequent to U–Pb and/or U–Th dating. The UCLA Cameca ims 1270 ion microprobe was tuned for high mass resolution analysis at a mass resolving power $M/\Delta M = 8,000$ (at 10% peak height), sufficient to largely resolve interferences such as $^{48}Ca^{+}$ and $^{96}Zr^{2+}$. A ~ 10 nA $^{16}O^{-}$ primary beam was focused to a ~ 10 μm spot, and following a 120-s pre-sputter period with a 10 μm × 10 μm raster to minimize surface contamination, $^{48}Ti^{+}$ and $^{28}SiO^{+}$ intensities were measured simultaneously for 60 s using two electron multipliers. Ti concentrations were calculated using relative sensitivity factors determined on SL13 zircon (6.32 ± 0.33 ppm Ti; Harrison and Schmitt 2007). External reproducibility of Ti/Si relative sensitivity is estimated from replicate analyses on NIST 610 glass over a 2-day analysis period, which yielded a standard deviation of $\sim 1\%$ (relative; $n = 10$). All sputter pits were inspected for beam overlap on inclusions or adherent glass using a petrographic microscope, and only results for spots that were entirely contained within zircon are reported here (Tables 4, 5).

Results

Feldspar and obsidian $^{40}Ar/^{39}Ar$ eruption ages

$^{40}Ar/^{39}Ar$ ages for eight Pleistocene domes, sampling four of the seven previously defined eruption groups, are summarized in Table 2 (Fig. 2a–d and Appendix). The $^{40}Ar/^{39}Ar$ dating confirms that most silicic extrusions at Coso occurred in the range ~ 600 to ~ 60 ka, in general similar to that reported by previous K–Ar studies, but provides substantially better temporal resolution among individual eruptions. Sanidine from two samples from dome 28 (Group 2) the "Devils Kitchen" rhyolite was dated. Multi-grain step-heated sanidine analyses yield isochron ages of 611 ± 6 ka (all reported errors are given at 1σ or 68% confidence unless stated otherwise) ($^{40}Ar/^{36}Ar_0 = 297 \pm 3$, MSWD = 0.6) and 612 ± 7 ka ($^{40}Ar/^{36}Ar_0 = 296 \pm 11$, MSWD = 1.1) for samples PRCO-5 and PRCO-6, respectively. Multi-grain total fusion sanidine analyses yield isochron ages of 606 ± 7 ka ($^{40}Ar/^{36}Ar_0 = 305 \pm 5$, MSWD = 1.2) and 618 ± 7 ka ($^{40}Ar/^{36}Ar_0 = 299 \pm 12$, MSWD = 1.0), for samples PRCO-5 and PRCO-6, respectively. All 23 measurements
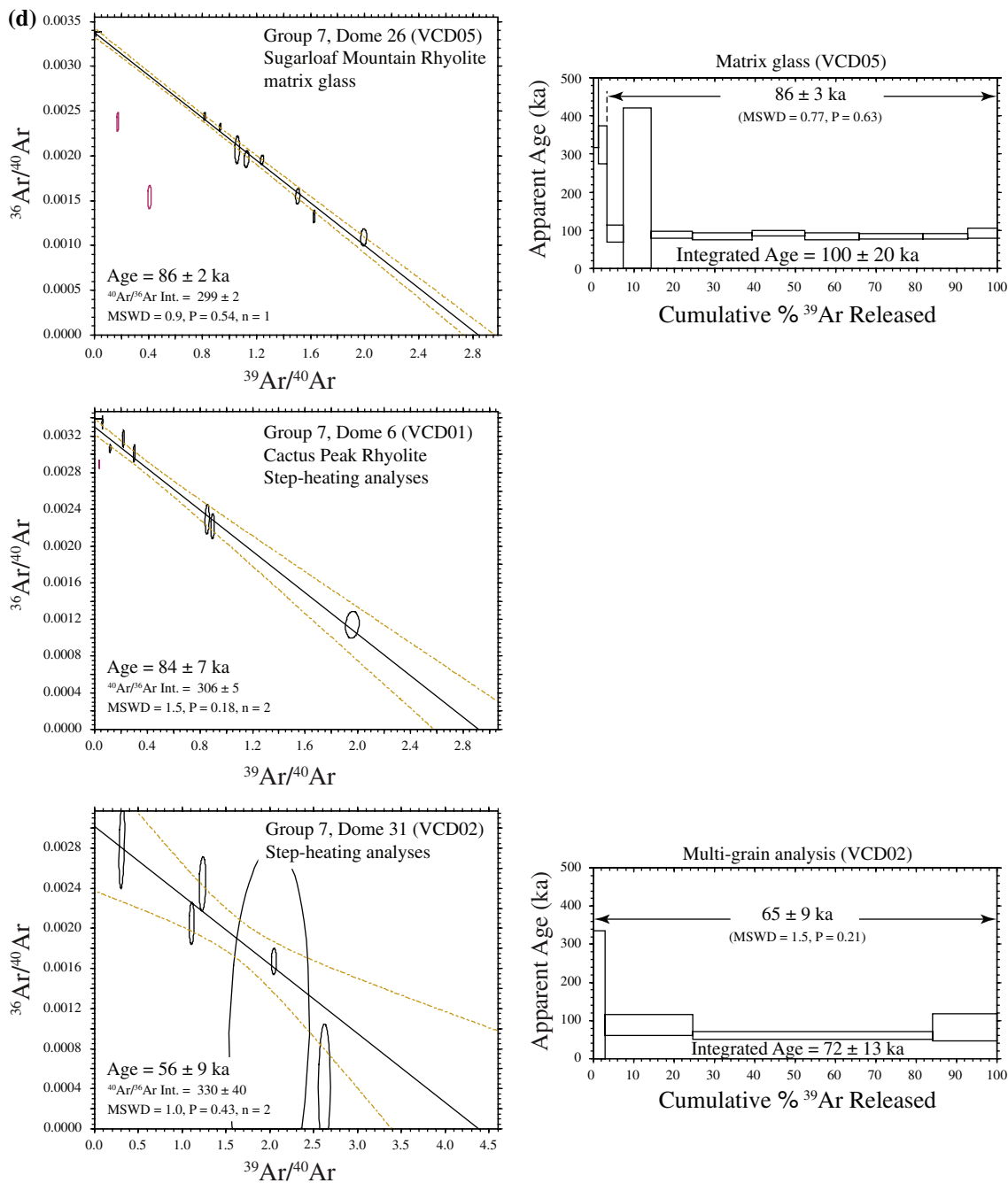
Fig. 2 continued

(step-heating and total fusion) from both Devils Kitchen rhyolite samples considered together yield an isochron age of 613 ± 6 ka ($^{40}Ar/^{36}Ar_0$ = 298 ± 2, MSWD = 0.9) that is within error of, but more precise than, the reported 587 ± 18 ka K–Ar date (Duffield et al. 1980).

Three samples were dated from dome 5 (Group 4), the northern most Pleistocene rhyolite at Coso. Seven separate multi-grain sanidine isochron ages for sample VCD03 range from ∼204 to ∼240 ka. An isochron fit to the combined data (Fig. 2b) reveals scatter toward greater $^{40}Ar/^{36}Ar_0$

isotope ratios that are consistent with presence of excess ^{40}Ar. Variable proportions of excess and atmospheric ^{40}Ar preclude the applicability of isochrons, which require a binary mixture of components. To mitigate this problem, individual analyses with comparatively high $^{40}Ar/^{36}Ar_0$ were incrementally excluded from below the inverse isochron until a sufficiently high probability of fit (0.1) was obtained. The resultant isochron age is 216 ± 6 ka ($^{40}Ar/^{36}Ar_0$ = 296 ± 13, MSWD = 1.5), which is ∼45 ka older than the nominal age for Group 4 rhyolites and

Table 2 $^{40}Ar/^{39}Ar$ eruption ages for select Pleistocene Coso rhyolites

Sample	Chemical group[a]	Material[b]	Age (ka)[c]	±1σ	$^{40}Ar/^{36}Ar$ Int.	±1σ	MSWD	p	n	Steps[d]
Dome 5	4									
VCD03		Glass	255	4	303	7	5.1	0.00	1	14
VCD03		Sanidine	216	6	296	13	1.5	0.10	6	19/25
PRCO-2		Sanidine	219	6	283	6	1.0	0.46	8	25/27
PRCO-2		Sanidine	217	9	292	5	1.6	0.20	4	–
PRCO-3		Sanidine	214	4	292	2	1.5	0.08	7	21
RCO-3		Sanidine	215	4	298	3	0.8	0.36	3	–
		Sanidine	**215**	**3**	**293**	**2**	**1.2**	**0.13**	**28**	**72/80**
Dome 6 (Cactus Peak)	7									
VCD01		**Sanidine**	**84**	**7**	**306**	**5**	**1.5**	**0.18**	**2**	**7/8**
Dome 24	6									
VCD08		**Sanidine**	**115**	**4**	**309**	**7**	**0.2**	**0.95**	**2**	**8/13**
Dome 25	6									
VCD09		**Sanidine**	**117**	**6**	**297**	**5**	**0.4**	**0.74**	**2**	**5/8**
Dome 26 (Sugarloaf Mt.)	7									
VCD05		**Glass**	**86**	**2**	**299**	**2**	**0.9**	**0.54**	**1**	**9/11**
Dome 28 (Devils Kitchen)	2									
PRCO-5		Sanidine	611	6	297	3	0.6	0.95	7	30/31
PRCO-5		Sanidine	606	7	305	5	1.2	0.31	5	–
PRCO-6		Sanidine	612	7	296	11	1.1	0.38	7	32
PRCO-6		Sanidine	618	7	299	12	1.0	0.37	4	–
		Sanidine	**613**	**6**	**298**	**2**	**0.9**	**0.71**	**23**	**71/72**
Dome 31	7									
VCD02		**Sanidine**	**56**	**9**	**330**	**40**	**1.0**	**0.43**	**2**	**6/8**
Dome 36										
VCD07	6	**Anorthoclase**	**148**	**6**	**296**	**2**	**0.2**	**1.00**	**5**	**17**

Bold indicates preferred age; for several measurements the first step or two that lie well below the best-fit isochron have been excluded and are assumed to reflect early degassing with Ar* contamination (see text)

MSWD mean sum of weighted deviates, p probably of fit to isochron, n number of analyses, where $n > 1$ indicates number of analyses combined in isochron age

[a] Eruptive groups after Bacon et al. (1981)

[b] Alkali feldspar distinction is based on measured K/Ca ratio (sanidine typically >10 and anorthoclase <5)

[c] Ages uncorrected for decay constant error, cf. Renne et al. (1998; see text)

[d] Heating steps

significantly older than its existing 170 ± 11 ka K–Ar date (Bacon et al. 1981). This model age is supported by sanidine measurements from the two other samples of dome 5 (PRCO-2 and PRCO-3) that yield multi-grain step-heating isochron ages of 219 ± 6 ka ($^{40}Ar/^{36}Ar_0 = 283 ± 6$, MSWD = 1.0) and 214 ± 4 ka ($^{40}Ar/^{36}Ar_0 = 292 ± 2$, MSWD = 1.5), respectively. Multi-grain total fusion sanidine analyses yield isochron ages of 217 ± 9 ka ($^{40}Ar/^{36}Ar_0 = 292 ± 5$, MSWD = 1.6) and 215 ± 4 ka ($^{40}Ar/^{36}Ar_0 = 298 ± 3$, MSWD = 0.8), for samples PRCO-5 and PRCO-6, respectively. If all 28 measurements (step-heating and total fusion) from all three dome 5 samples are considered together an isochron age of 215 ± 3 ka ($^{40}Ar/^{36}Ar_0 = 293 ± 2$, MSWD = 1.2) is determined. The

significance of the systematically subatmospheric trapped $^{40}Ar/^{36}Ar_0$ ratios for these two samples is unclear, but may derive from cosmogenic ^{36}Ar (Renne et al. 2001) accumulated in these exposed surface samples.

The three dated southern domes are older than their reported mean Group 6 age of ∼90 ka. It is probable that the anomalously young K–Ar dates reflect incomplete extraction of Ar from feldspar and other phases contained in the analyzed obsidian. Domes 24 (VCD08) and 25 (VCD09) yield similar multi-grain feldspar isochron ages of 115 ± 4 ka ($^{40}Ar/^{36}Ar_0 = 309 ± 7$, MSWD = 0.2) and 117 ± 6 ka ($^{40}Ar/^{36}Ar_0 = 297 ± 5$, MSWD = 0.4) that are nominally 30–40 ka older than their reported 84 ± 32 and 86 ± 24 ka K–Ar ages (Lanphere et al. 1975),

Table 3 U–Th isotope results and ^{238}U–^{230}Th ages for Coso allanites

Sample	$(^{230}Th)/(^{232}Th)^a$	±1σ	$(^{238}U)/(^{232}Th)^a$	±1σ	U (ppm)	Th (ppm)	Model age (ka)	+1σ	−1σ
Lavas									
Dome 6 (VCD01)	0.883	0.002	0.878	0.001	7.32	25.29	–	–	–
Dome 24 (VCD08)	0.887	0.002	0.802	0.001	5.85	22.12	–	–	–
Dome 26 (VCD05)	0.838	0.002	0.883	0.001	7.15	24.59	–	–	–
Allanites									
Dome 6 (Cactus Peak)									
VCD01_r2g1s1	0.426	0.039	0.01502	0.00008	–	–	82	11	10
VCD01_r2g1s2	0.431	0.033	0.01427	0.00009	–	–	81	9	8
VCD01_r2g3s1	0.461	0.033	0.01637	0.00010	–	–	73	9	8
VCD01_r2g4s1	0.414	0.026	0.01555	0.00007	–	–	86	7	7
VCD01_r2g6s1	0.414	0.030	0.01787	0.00007	–	–	86	9	8
VCD01_r3g2s1	0.368	0.028	0.01825	0.00009	–	–	100	9	9
VCD01_r3g5s1	0.066	0.010	0.02082	0.00008	–	–	334	32	25
Dome 24									
VCD08_r29g1s1	0.385	0.035	0.0247	0.0001	–	–	113	15	13
VCD08_r29g1s2	0.377	0.043	0.0204	0.0001	–	–	115	19	16
VCD08_r30g1s1	0.375	0.037	0.0226	0.0002	–	–	117	16	14
VCD08_r33g1s1	0.335	0.058	0.0213	0.0002	–	–	134	32	25
Dome 26 (Sugarloaf)									
VCD05_r4g3s1	0.362	0.026	0.01485	0.00006	–	–	87	8	7
VCD05_r5g7s	0.010	0.006	0.01138	0.00007	–	–	327	17	15

Analyses are identified by row (r#), grain (g#), spot (s#)

[a] Activity ratios

respectively. Both composite isochrons are composed of two separate multi-grain sanidine step-heating analyses. In total, the four separate isochrons range in age from ∼113 to ∼119 ka. For the third previously undated Group 6 dome (dome 36, VCD07), an isochron populated with five multi-grain anorthoclase step-heating analyses yields an age of 148 ± 6 ka ($^{40}Ar/^{36}Ar_0 = 296 ± 2$, MSWD = 0.2). The separate multi-grain anorthoclase isochron ages range from ∼141 to ∼160 ka.

Analyses of three Group 7 samples suggest that eruptions in this group appear to have occurred in (at least) two events. The small previously undated dome 31 (VCD02) from the northern part of the Coso field yields a multi-grain step-heated sanidine isochron age of 56 ± 9 ka ($^{40}Ar/^{36}Ar_0 = 330 ± 40$, MSWD = 1.0). Individual multi-grain analyses (also used in the composite isochron age) yield a plateau age of 66 ± 5 ka MSWD = 1.5 (see Fig. 2d). Although the data are sparse, we believe that the eruption age of dome 31 is similar to the reported ∼60 ka age of Group 7 rhyolites. Coeval eruption of Sugarloaf and Cactus Peak domes, however, appear to have occurred at ∼86 ka: ∼40 ka later and ∼15 ka earlier, respectively, than their K–Ar dates would indicate (Lanphere et al. 1975). Step-heating analyses of glass from Sugarloaf dome 26 (VCD05) gives an isochron

age of 86 ± 2 ka ($^{40}Ar/^{36}Ar_0 = 299 ± 2$, MSWD = 0.9) and multi-grain step-heating analyses of sanidine from Cactus Peak dome 6 (VCD01) yield a combined isochron age of 84 ± 7 ka ($^{40}Ar/^{36}Ar_0 = 306 ± 5$, MSWD = 1.5). Considered separately, the two multi-grain step-heating analyses of Cactus Peak sanidine yield isochron ages of ∼86 and ∼96 ka, respectively. Obsidian from four Coso domes, including domes 17 and 20, in which there was insufficient feldspar for dating, and dome 6 (Cactus Peak) and dome 31, which were dated by feldspar, contain largely atmospheric Ar (>50 to 99%) and provide no reliable age information.

U–Th isotope results and ^{238}U–^{230}Th allanite and zircon model crystallization ages

The ^{238}U–^{230}Th–^{232}Th compositions of allanite, zircon, their associated lavas, and zircon from the granophyre cuttings sample, as well as ^{238}U–^{230}Th model ages of zircon and allanite (see Reid et al. 1997), are listed in Tables 3 and 4. Approximately 50% of all of the zircons dated (n = 43) in this study yielded ^{238}U–^{230}Th results within error of secular equilibrium and these were reanalyzed for their ^{238}U–^{206}Pb ages (see Table 5). Representative secondary electron and cathodoluminescence images of analyzed zircon and allanite

Table 4 U–Th isotope results and ^{238}U–^{230}Th ages for Coso zircons

Sample	$(^{230}Th)/(^{232}Th)^a$	±1σ	$(^{238}U)/(^{232}Th)^a$	±1σ	U (ppm)	Th (ppm)	Ti (ppm)[b]	Model age (ka)	+1σ	−1σ
Zircons										
Dome 6 (Cactus Peak)										
VCD01_r2g3s1	3.61	0.13	3.53	0.02	1,035	930		∞	–	–
VCD01_r2g5s1	2.63	0.15	2.62	0.02	586	710		∞	–	–
VCD01_r3g10s1	3.50	0.09	5.80	0.02	3,100	1,693		83	4	4
VCD01_r6g1s1	3.24	0.08	5.29	0.04	2,616	1,546	2.7	83	5	4
VCD01_r6g4s1	3.04	0.06	5.13	0.03	6,551	4,046		77	4	4
VCD01_r6g7s1	4.26	0.16	7.17	0.01	1,498	649		84	6	6
VCD01_r7g7s1	4.11	0.59	4.11	0.09	154	119		∞	–	–
VCD01_r7g8s1	3.29	0.16	3.24	0.01	583	571		∞	–	–
Dome 26 (Sugarloaf)										
VCD05_r2g5s1	2.27	0.19	2.33	0.02	277	372		470	–	267
VCD05_r2g6s1	8.21	0.46	7.96	0.05	377	148		∞	–	–
VCD05_r4g5s1	4.09	0.20	3.95	0.08	497	394		∞	–	–
VCD05_r4g7s1	4.03	0.16	6.09	0.01	1,312	572		104	9	8
VCD05_r6g8s1	3.01	0.17	3.12	0.01	302	304		386	–	141
VCD05_r7g5s1	1.74	0.05	1.71	0.02	1,634	2,996		∞	–	–
Well 46A-19RD										
Coso_up_g5s1	6.24	0.21	7.35	0.11	2,119	896		193	27	22
Coso_p_g1s1	5.53	0.09	6.30	0.10	2,413	1,191	1.1	213	23	19
Coso_p_g4s1	5.55	0.16	6.34	0.22	1,392	683	2.7	211	55	36
Coso_p_g5s1	5.64	0.20	6.32	0.19	255	126	2.8	226	64	40
Coso_p_g6s1	4.18	0.09	5.01	0.06	1,568	974	2.6	175	16	14
Coso_p_g7s1	3.40	0.30	3.56	0.11	33	29		304	–	120
Coso_p_g8s1	2.66	0.06	3.06	0.04	1,137	1,158	3.7	184	21	18
Coso_p_g9s1	3.53	0.07	4.11	0.05	1,188	900	1.8	187	18	16
Coso_p_g9s2	3.87	0.08	4.53	0.05	1,243	854		187	19	16
Coso_p_g10s1	1.79	0.05	1.79	0.03	192	333		∞	–	–
Coso_p_g10s2	1.53	0.05	1.60	0.03	169	328		246	209	67

Analyses are identified by unpolished surface (up), polished (p), row (r#), grain (g#), spot (s#). ∞ Indicates secular equilibrium; age is >350 ka

[a] Activity ratios

[b] Used for Ti-in-zircon temperature (see text)

are shown in Fig. 3. Using whole rock compositions to account for initial ^{230}Th/^{232}Th during crystallization (Reid et al. 1997), allanites from dome 24 (VCD08) yield model ^{238}U–^{230}Th ages that cluster at ∼115 ka, whereas allanites from Cactus Peak (dome 6, VCD01) and Sugarloaf (dome 26, VCD05) give ages that cluster around ∼85 ka. Two allanites yield ages that are >300 ka, one each from the Cactus Peak and the Sugarloaf rhyolites. Excluding the >300 ka crystal, Cactus Peak allanites yield a weighted mean ^{238}U–^{230}Th model age of 85 ± 10 ka (95% CI, $n = 6$, MSWD = 1.0), and a Sugarloaf allanite gives a model age of 86 ± 8 ka (Fig. 4a). The four Cactus Peak zircons give a weighted mean ^{238}U–^{230}Th model age of 81 ± 7 ka (95% CI, $n = 4$, MSWD = 0.5) that is indistinguishable in age from the coexisting allanites as well as the eruption age measured by ^{40}Ar/^{39}Ar dating. A zircon from Sugarloaf

yields an older model ^{238}U–^{230}Th age of 104 ± 9 ka (Fig. 4a). Based on their similar trace element concentrations (Bacon et al. 1981) and ^{40}Ar/^{39}Ar ages of the rhyolites (Table 2), the allanite and zircon model ages may be grouped. A combined weighted mean model age for zircons and allanites from Cactus Peak and Sugarloaf rhyolites (domes 6 and 26) is 83 ± 8 ka (95% CI, $n = 12$, MSWD = 1.0). A combined internal isochron ^{230}Th/^{232}Th–^{232}Th/^{238}U age for the allanite and zircon from domes 6 and 26 is 84 ± 4 ka (2 σ, $n = 12$, MSWD = 1.0, Fig. 5). The U/Th ratio of the allanites shows a twofold variation of 0.0036 to 0.0074 that does not correlate with ^{238}U–^{230}Th model age (see Fig. 4a).

Allanites from dome 24 (VCD08, Group 6) yield a weighted mean age of 117 ± 44 ka (95% CI, $n = 4$, MSWD = 0.2) and exhibit variation in the U/Th ratio of

Table 5 U–Pb isotope compositions and zircon ages

Sample	$^{206}Pb/^{238}U$	$\pm1\sigma$	$^{207}Pb/^{235}U$	$\pm1\sigma$	$^{207}Pb/^{206}Pb$	$\pm1\sigma$	$^{206}Pb/^{238}U$ age (Ma)	$\pm1\sigma$	U (ppm)	Th (ppm)	Ti (ppm)[b]
Dome 6 (Cactus Peak)											
VCD01_r2g2s1	0.0089	0.0011	0.0637	0.0079	0.052	0.001	57	7	1,008	916	
VCD01_r2g5s2	0.0248	0.0019	0.1666	0.0132	0.049	0.001	158	12	48	32	
VCD01_r2g7s1	0.0169	0.0016	0.1172	0.0111	0.050	0.001	108	10	177	243	
VCD01_r2g9s1	0.0004	0.0000	0.042	0.0036	0.780	0.020	[a]	–	697	340	2.9
VCD01_r7g4s1	0.0001	0.000006	0.0057	0.0006	0.720	0.020	[a]	–	2,195	1,219	
VCD01_r7g7s2	0.0156	0.0012	0.1079	0.0086	0.050	0.001	100	8	154	119	
VCD01_r7g8s2	0.0228	0.0020	0.1811	0.0158	0.058	0.001	145	13	229	97	
Dome 26 (Sugarloaf)											
VCD05_r2g3s1	0.0001	0.00001	0.0085	0.0014	0.590	0.080	[a]	–	183	106	
VCD05_r2g4s2	0.0229	0.0013	0.1667	0.0098	0.053	0.001	146	8	177	266	
VCD05_r2g6s2	0.0149	0.0005	0.1007	0.0033	0.049	0.001	95	3	550	293	
VCD05_r3g1s1	0.0001	0.000004	0.0079	0.0005	0.760	0.020	[a]	–	2,451	1,118	
VCD05_r3g3s1	0.0253	0.0005	0.1965	0.005	0.056	0.001	161	3	319	129	
VCD05_r3g5s1	0.0227	0.0005	0.1615	0.0063	0.052	0.002	145	3	126	104	
VCD05_r3g6s1	0.0248	0.0004	0.1752	0.0029	0.051	0.000	158	2	972	910	
VCD05_r4g1s1	0.0012	0.0002	0.1257	0.0184	0.750	0.030	[a]	–	2,617	1,207	
VCD05_r4g2s1	0.0261	0.0005	0.1954	0.0044	0.054	0.001	166	3	265	201	
VCD05_r4g4s1	0.0235	0.0006	0.1464	0.0102	0.045	0.003	150	4	40	37	
VCD05_r4g5s2	0.0304	0.0010	0.2268	0.0083	0.054	0.001	193	6	497	334	
VCD05_r4g6s1	0.0003	0.0000	0.0307	0.0014	0.790	0.010	[a]	–	3,763	1,766	
VCD05_r4g7s1	0.0148	0.0003	0.0991	0.0022	0.049	0.001	94	2	766	377	
VCD05_r5g4s2	0.0002	0.0000	0.0234	0.0026	0.780	0.040	[a]	–	744	398	1.6
VCD05_r5g5s1	0.0003	0.0001	0.0343	0.0066	0.760	0.040	[a]	–	6,041	3,225	
VCD05_r5g7s1	0.0283	0.0005	0.2048	0.0051	0.053	0.001	180	3	267	219	
VCD05_r6g1s1	0.0316	0.0007	0.2226	0.0063	0.051	0.001	200	4	96	41	
VCD05_r6g3s1	0.0252	0.0006	0.1827	0.0045	0.053	0.001	160	4	520	103	
VCD05_r6g8s2	0.0236	0.0007	0.1675	0.0056	0.052	0.001	146	4	302	258	
VCD05_r7g5s2	0.0225	0.0009	0.1610	0.0065	0.052	0.001	144	5	1,634	2,536	
Well 46A-19RD											
Coso46A_up_g1	0.0002	0.000011	0.0206	0.0018	0.794	0.085	0.136	0.124	1,108	323	
Coso46A_up_g3	0.0298	0.0009	0.2619	0.0079	0.064	0.002	186	6	243	19	11.2
Coso46A_up_g4	0.000022	0.000002	0.00096	0.00018	0.315	0.059	0.181	0.014	2,318	544	
Coso46A_up_g5	0.000022	0.000002	0.00043	0.00011	0.139	0.034	0.213	0.012	3,123	796	
Coso1_p_g2	0.0268	0.0009	0.1922	0.0108	0.052	0.002	170	5	399	388	8.2
Coso1_p_g5	0.000030	0.000002	0.00166	0.00022	0.405	0.053	0.178	0.018	1,863	724	
Coso1_p_g7	0.0230	0.0010	0.1902	0.0148	0.060	0.004	145	7	71	38	9.0
Coso1_p_g8	0.000497	0.000065	0.0520	0.0065	0.759	0.054	0.344	0.556	2,335	1,247	
Coso1_p_g10	0.0253	0.0007	0.1762	0.0062	0.051	0.001	160	4	530	644	17.9

Analyses are identified by unpolished surface (up) or polished (p) or row (r#), grain (g#), spot (s#). Uncertainties are 1σ

[a] No age assigned to grains with $^{207}Pb/^{206}Pb$ >0.6

[b] Used for Ti-in-zircon temperature (see text)

0.0054 to 0.0079 (Fig. 4b). Allanite from dome 24 is indistinguishable in age from the time of eruption as determined by $^{40}Ar/^{39}Ar$ dating.

The granophyre sample is altered and consists of drill cuttings, and therefore it is impossible to reliably determine its whole rock ^{238}U–^{230}Th isotope composition. Using the

Fig. 3 Backscattered-electron (*BSE*, *left*) and cathodoluminescence or secondary electron (*CL/SE*, *right*) images of dated accessory minerals. I: Representative image of subhedral to anhedral Pleistocene zircon. II: Representative image of euhedral Mesozoic zircon. III: Representative image of subhedral to anhedral allanite. *A* allanite, *G* glass, *Z* zircon, *cpx* clinopyroxene
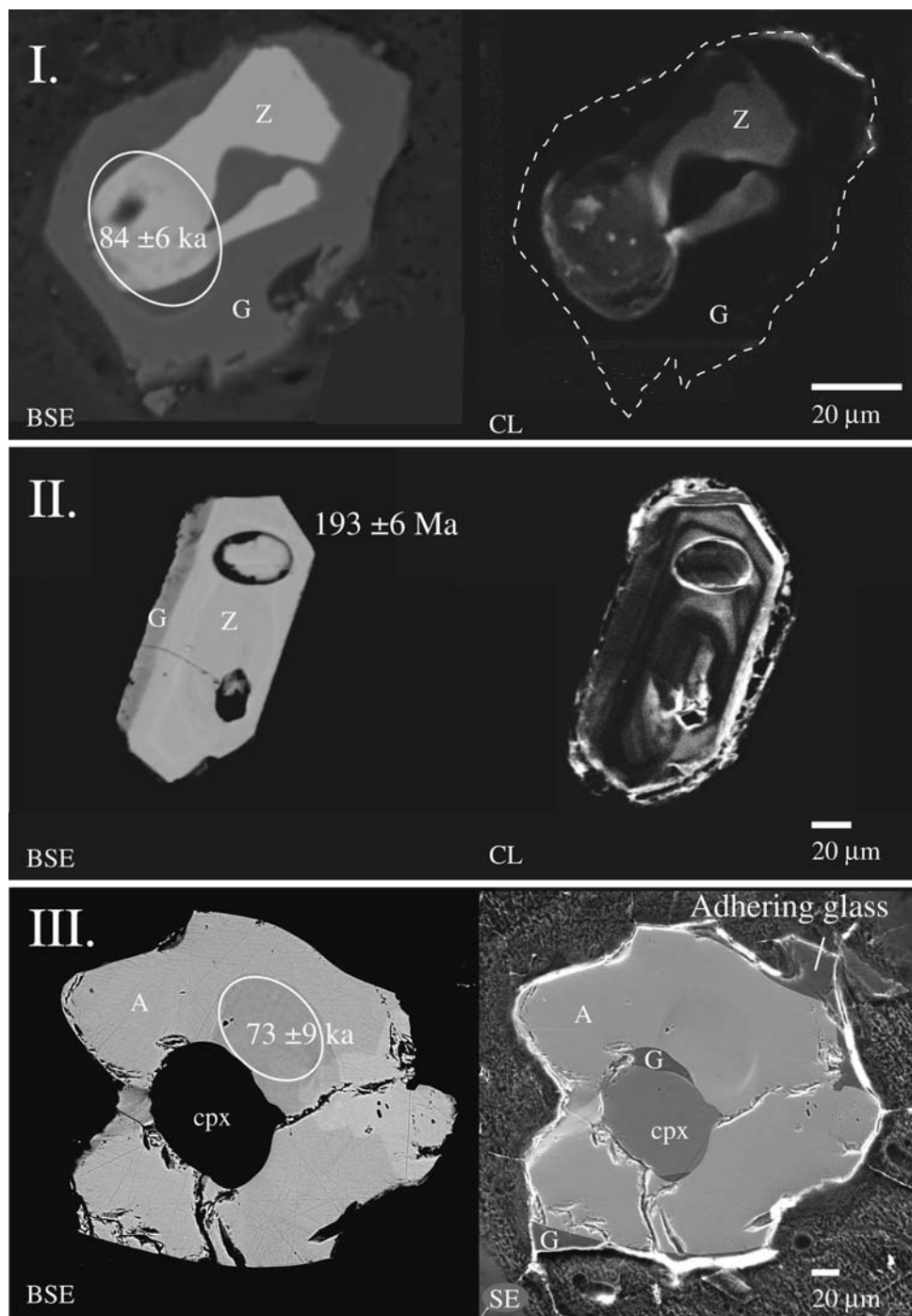
whole rock ^{238}U–^{230}Th composition of Cactus Peak rhyolite, zircon model ^{238}U–^{230}Th ages give a weighted mean age of 192 ± 11 ka (95% CI, $n = 9$, MSWD = 0.2; Fig. 4c). An internal isochron age of 218^{+60ka}_{-46ka} (95% CI, $n = 8$, MSWD = 0.57) is determined for the granophyre zircons. This age is less precise because of the limited spread in zircon Th/U ratios as compared to lava (melt)-zircon pairs, but overlaps with the weighted mean model age, which demonstrates that our assumptions related to host melt composition are reasonable (Fig. 5). The isochron age for the granophyre zircons is distinct from the zircon and allanite ages from the Group 7 rhyolites, but similar to the ∼215 ka $^{40}Ar/^{39}Ar$ eruption age of dome 5. Three zircons from the granophyre sample 46A-19D and five additional crystals from the lavas yield ^{238}U–^{230}Th in equilibrium. These crystals were dated by the U–Pb method (see Table 5).
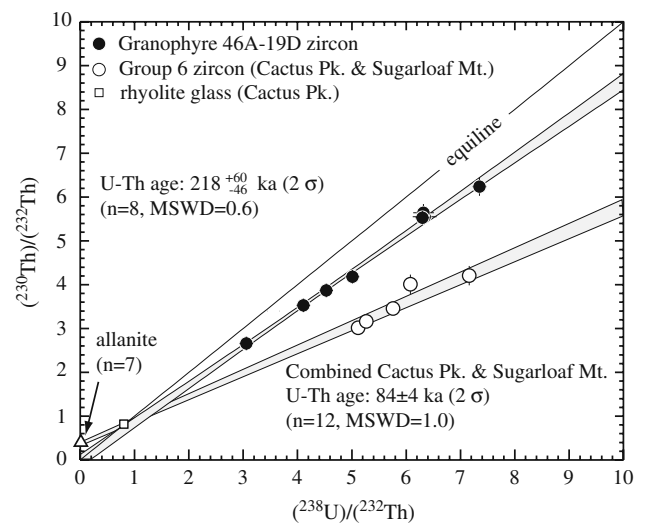
Fig. 5 Internal U–Th isochrons for zircon from granophyre drill cuttings and for zircons and allanites from Cactus Peak and Sugarloaf Mt. Symbols defined in figure. *Shaded error envelopes are 2σ*
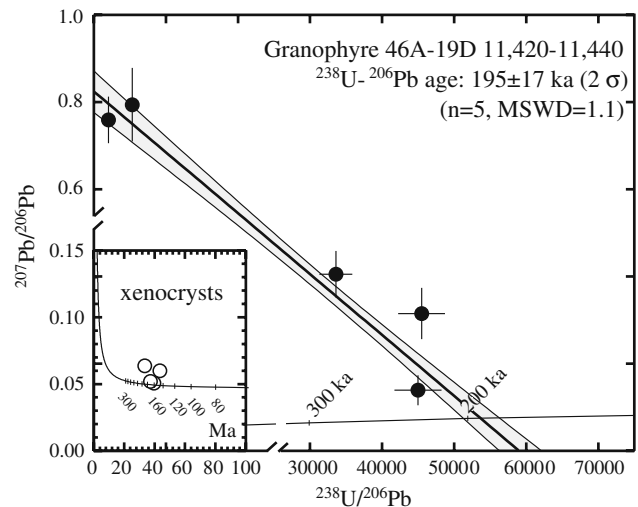
Fig. 4 ^{238}U–^{230}Th ages and $(^{238}U)/(^{232}Th)$ compositions for allanite and zircon from selected Coso rhyolites. **a** Cactus Peak and Sugarloaf rhyolites, **b** Dome 24, and **c** Granophyre drill core 46A-19RD. Symbols are defined in figure. Uncertainty of ion microprobe spot analyses are 1 σ. ^{40}Ar/^{39}Ar eruption ages (this study) included for reference. *Vertical shaded bands* show uncertainty for weighted mean ^{238}U–^{206}Pb (*dashed*) and ^{238}U–^{230}Th isochron (*dot-dashed*) ages for Pleistocene zircon from the granophyre

U–Pb isotope results and ^{238}U–^{206}Pb zircon crystallization ages

Many dated zircons exhibit Mesozoic ^{238}U–^{206}Pb ages (Table 5; Fig. 6). After correction for disequilibrium, Pleistocene zircons from the granophyre sample yield a weighted mean ^{238}U–^{206}Pb age of 195 ± 17 ka (95% CI, $n = 5$, MSWD = 1.1) that is in agreement with their ^{238}U–^{230}Th age (Figs. 4, 5). ^{238}U–^{206}Pb analysis of other zircon from Cactus Peak, Sugarloaf, and the granophyre sample 46A-19D (that were not analyzed for ^{238}U–^{230}Th) reveals grains with little radiogenic Pb (^{207}Pb/^{206}Pb ≥0.6) as well as grains that yield Mesozoic ages (Table 5). The

Fig. 6 Tera Wasserburg diagram showing ^{238}U–^{206}Pb zircon ages from granophyre drill core. *Error bars and shaded envelope are 1σ. Inset shows Mesozoic xenocrysts. Concordia shown corrected for initial U–Th disequilibrium*

Mesozoic zircons define a ^{238}U–^{206}Pb age distribution with peaks at ∼95 Ma, ∼145 to 155 Ma, and ∼180 to 200 Ma (Fig. 7). A single zircon analysis yields an age of ∼60 Ma. Zircons from granophyre cuttings have ages that fall within the older Mesozoic age groups, but their origin(s) remain ambiguous because of potential contamination from country rock during drilling.

Compositional zoning in dated allanite and zircon

The U/Th ratios of zircon interiors vary from ∼1.0 to ∼2.3 among those that exhibit clear ^{238}U–^{230}Th
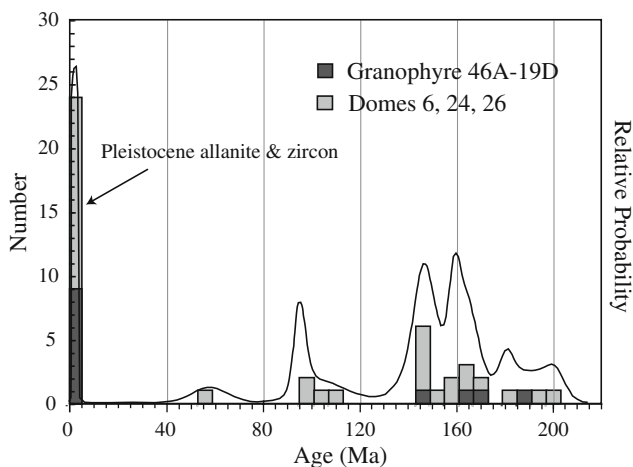
Fig. 7 Histogram and relative probability curve showing bimodal (Pleistocene and Mesozoic) accessory mineral age distribution for Coso domes 6, 24, 26 and granophyre

disequilibrium. This range is indistinguishable among the grains from the different extrusions and the granophyre. The U/Th ratios of the interior of the eight zircons that are in ^{238}U–^{230}Th equilibrium exhibit a greater range from ~0.5 to ~2.6. In general, unpolished surface analyses ("up" in Table 4) yield higher U/Th ratios that vary from ~2.4 to ~4.3 (in one case up to 12.6), indicating increasing U/Th during crystallization. Rimward enrichment of incompatible elements is consistent with magmatic zircon growth (e.g., Claiborne et al. 2006). The Pleistocene and Mesozoic zircons are zoned in backscatter-electron imaging as well as cathodoluminescence images (Fig. 3). The zircons display internal zoning that is truncated by thin rims. The Mesozoic zircons are commonly euhedral to subhedral, whereas the Pleistocene zircons are subhedral to anhedral. There is no observed grain size distinction between the two age populations. Backscattered-electron imaging reveals that individual Coso allanites are not significantly zoned (Fig. 3).

Ti-in-zircon thermometry

Zircon crystallization temperatures using Ti-in-zircon thermometry (Ferry and Watson 2007; Watson and Harrison 2005) were calculated from Ti abundances measured by ion microprobe (Tables 4, 5). Based on the presence of quartz in essentially all Coso rhyolites (Manley and Bacon 2000), granophyre 46A-19RD, as well as plutonic and metamorphic country rocks, model Ti-in-zircon temperatures assume silica activity (a_{SiO2}) = 1. Titania activities (a_{TiO2}) were estimated using: (1) the compositions of coexisting Fe–Ti oxides (cf. Wark et al. 2007) reported by Manley and Bacon (2000), and (2) the rutile saturation model of Hayden et al. (2006) using whole-rock

composition (Bacon et al. 1981) and the Watson and Harrison (1983) zircon saturation temperature. For Mesozoic xenocrysts a_{TiO2} was assumed to be unity. Pleistocene zircons from granophyre 46A-19RD and Cactus Peak and Sugarloaf Mt. rhyolites yield crystallization temperatures between 610 and 740°C, with averages of 690°C (for $a_{TiO2} = 0.41$) and 660°C (for $a_{TiO2} = 0.62$). In contrast, xenocrystic zircon Ti abundances are higher by at least a factor of 2, and their model crystallization temperatures range from 740 to 800°C (for $a_{TiO2} = 1$). These temperatures will be higher if a_{TiO2} is <1, as is typical for granitic magmas (Watson and Harrison 2005).

Discussion

The accuracy and concordance of eruption and pre-eruption ages of Coso rhyolites

Alkali feldspar phenocrysts are ideal for dating eruption of Quaternary rhyolites by the $^{40}Ar/^{39}Ar$ method. The young ages of the Coso rhyolites make their $^{40}Ar/^{39}Ar$ analysis insensitive to the interpreted age bias due to ^{40}K decay constant errors (i.e., Min et al. 2000). The exception is the 623 ± 6 ka Devils Kitchen rhyolite that after correction is ~10 ka older than measured (i.e., 613 ka). Faced with the possibility of insufficient $^{40}Ar*$ in single crystals we chose to perform replicate multi-grain total fusion and step-heating analyses. In some cases excess $^{40}Ar*$ due to trapped melt inclusions or partially degassed xenocrysts (cf. Ton-That et al. 2001) may complicate interpretation of the results, as appears to be the case for feldspar from sample VCD03, one of three samples dated from dome 5. As explained above, to mitigate this problem step-heating data were deleted stepwise from below the inverse isochron until a reasonably high probability of fit (0.1) was obtained. The resultant isochron age of 215 ± 6 ka is indistinguishable from the ~214 to 220 ka isochron ages determined for the other two dome 5 samples.

For those Coso rhyolites where obsidian is present, non-hydrated glass may be dated by $^{40}Ar/^{39}Ar$, as was previously done using K–Ar methods (Duffield et al. 1980; Lanphere et al. 1975). Excess Ar due to open system evolution (i.e., consistent with the existence of old zircon and allanite ages) may explain the difference between the glass date of ~255 ka for dome 5 (VCD-03; Table 2) and the ~215 ka feldspar ages. Notably, the inverse isochron fit to the glass data reveals excess scatter as indicated by an MSWD of 5.1. The problematic glass data likely reflect excess $^{40}Ar*$ and/or atmospheric contamination possibly coupled with kinetic fractionation of Ar isotopes during disequilibrium exchange between atmospheric and magmatic reservoirs. Alternatively, it may have experienced

cryptic secondary mobility of K and Ar due to hydration, although this is considered to be less likely (Morgan et al. 2007). In contrast, step-heating analyses of glass from Sugarloaf Mountain dome 26 (VCD05) define a well-behaved inverse isochron that yields an age of 86 ± 2 ka with a MSWD of 0.9. This age is indistinguishable from Sugarloaf Mountain dome allanite model age of ~86 ka and the Cactus Peak allanite model age of ~85 ka. The glass ^{40}Ar/^{39}Ar age is also consistent with the ~84 ka internal U/Th isochron age calculated from zircon and allanite (Fig. 5).

There is excellent agreement between the ^{40}Ar/^{39}Ar and the U–Th–Pb accessory mineral dating for individual rhyolites performed in this study (Fig. 4a, b). In contrast, the 623 ± 6 ka ^{40}Ar/^{39}Ar eruption age from the two Devils Kitchen samples appears older than the youngest zircon ("rim") dates reported for the Devils Kitchen rhyolite by Miller and Wooden (2004) that appear to exhibit a bimodal age distribution with the younger maximum at ~550 ka. A similar discrepancy exists between the 587 ± 18 ka K–Ar date reported by Duffield et al. (1980) and the youngest zircon rim dates that because of this difference was considered unreliable by Miller and Wooden (2004). Regardless, Miller and Wooden (2004) provide compelling evidence from the zircon ("core") measurements that crystallization initiated at least ~150 ka prior to the eruption. A majority of the reported zircon rim ages (n = 19/21) are within error (1 σ) of and define a "broad hump" that straddles the 623 ± 6 ka ^{40}Ar/^{39}Ar date, although it is unclear whether the reported age range for the rim measurements originates from analytical or geological variability. The youngest zircon core ages (Miller and Wooden 2004) are noteworthy because they are in excellent agreement with the new ^{40}Ar/^{39}Ar eruption age determination. The apparent bimodal age distribution of the zircon "rim" measurements reported by Miller and Wooden (2004) may be spurious due to the fact that uncertainties related to Th and U abundances in the concentration standard used and the assumed melt composition for the initial U–Th disequilibrium correction were not propagated into the reported errors. The latter point deserves further explanation: it is conceivable that a less evolved component contaminated the melt shortly prior to eruption without permitting significant zircon growth. This scenario is supported by the abundant mafic enclaves in the Devils Kitchen rhyolite (Bacon and Metz 1984). Based on such a scenario and the range of potential mafic magma and hybridized inclusion compositions reported at Coso (e.g., Bacon and Metz 1984), the U/Th ratio of the rhyolite compositions in which the zircon grew could have been different than measured. If addition of a relatively high-U/Th component occurred then this could make the reported zircon ages for the Devils Kitchen rhyolite too young.

Notably, the whole rock uranium concentrations measured in this study are approximately half those expected for the younger rhyolites and therefore the actual abundance in Devils Kitchen may also be lower. Because of this possibility; i.e., that the assumed U/Th ratio for the melt from which the zircon crystallized may be too high, the zircon ages could be an extra ~5 ka too young. In addition, this age discrepancy may be due, in part, to a ^{230}Th excess related to the melt generation process, i.e., derived from a zircon bearing mush or wall-rock based on the uranium-series disequilibrium measured in this study for the younger rhyolites.

The Pleistocene zircon ages (~200 ka) from the sub-surface granophyre sample demonstrate that magma was emplaced into the shallow crust at the time, close to extrusion of dome 5 at ~215 ka. Based on the measured zircon age uncertainties it is conceivable that magma that ultimately became the granophyre was related to Group 3 or 4 extrusions, possibly either as a proximal intrusive body or a residual crystal mush. Nevertheless, the narrow zircon age span (≤20 ka) observed in the granophyre indicates that it likely crystallized rapidly and therefore probably represents a short-lived magma body.

Significance of bimodal zircon age populations in Coso rhyolites

The Devils Kitchen rhyolite contains by far the greatest crystal content and the most enclaves of any Coso rhyolite (Bacon et al. 1981). The porphyritic mafic enclaves themselves are contaminated with gabbroic and alkali-granitic crystal mush and show evidence of commingling at mafic and rhyolite magma contacts (Bacon and Metz 1984). These observations, along with the fact that the Devils Kitchen contains Quaternary zircons that significantly pre-date eruption (Miller and Wooden 2004) suggest that this low-temperature rhyolite reflects eruption of a near solidus magma and/or crystals liberated from Quaternary intrusions rejuvenated, perhaps episodically, by mafic influx (Bacon and Metz 1984; Miller and Wooden 2004). The incorporation of mafic enclaves into the Devils Kitchen magma likely occurred shortly before its eruption.

Disequilibrium features are common to all Coso rhyolites. However the salient features of the Devils Kitchen rhyolite contrast strongly with the crystal-poor (<2%) nature of the younger rhyolites. The abundance of Meso-zoic zircon observed in the younger rhyolites (this study) and their absence in the Devils Kitchen rhyolite reinforces this distinction. If the younger rhyolites were directly differentiated from any residual Devils Kitchen magma, then sufficient time or thermal energy would be needed to dissolve the inherited zircon (e.g., Watson and Harrison 1983). Recycling might represent adjustment of the magma

reservoir margins near the time of eruption. Any widening of the conduits or reservoir may have led to the introduction of zircon xenocrysts from Mesozoic wall-rocks. Alternatively, the younger rhyolites may represent transient and discrete magma bodies that interacted with country rock. In this case, the younger rhyolites reflect discrete batches of fresh highly-evolved rhyolitic magma that not only require extensive fractional crystallization, but also involve melting and/or assimilation of local country rocks and then rapid eruption.

The narrow age range of Quaternary zircon along with the abundant Mesozoic zircons present in the granophyre (46A-19D) resemble the bimodal zircon age populations observed in the Cactus Peak and Sugarloaf Mt. rhyolites, and imply that: (1) the intrusion formed independently from the Devils Kitchen rhyolite, or (2) that by $\sim$215 ka all of the Devils Kitchen-related residual crystal mush was processed (i.e., excluded from the younger magmas because it was erupted, dissolved, or crystallized). It is possible that the Mesozoic zircons in the granophyre represent contamination during the drilling through overlying wall-rock. Hence, the Mesozoic zircons cannot be unambiguously interpreted as magmatic xenocrysts.

The Coso rhyolites are unusual among silicic extrusions in that a majority of their zircons are clearly xenocrysts derived from the much older wall-rocks of the magmatic system. In other rhyolites (e.g., Bachmann et al. 2007), widely distributed ages for zircons make distinctions between autocrysts, xenocrysts, and antecrysts ambiguous (e.g., Charlier et al. 2005). Classic inheritance (sensu Gulson and Krogh 1973) in several silicic extrusions has been identified by ion microprobe spot analyses of crystal cores, e.g., in crystal-rich units like the Tertiary Amalia Tuff of New Mexico (Johnson et al. 1989), the Fish Canyon Tuff of Colorado (Lanphere and Baadsgaard 2001), and the $\sim$1.2 Ma Ongatiti ignimbrite from the Taupo volcanic zone, New Zealand (Brown and Smith 2004). Similar evidence for the incorporation of basement material also exists for a couple crystal-poor units at Taupo (the $\sim$20 ka unit Ω and 6–7 ka unit G; Charlier et al. 2005). Unit Ω largely contains Pleistocene zircon and exhibits less than $\sim$15% basement aged zircon—much less abundant than the $\sim$50% or more found in the post-230 ka Coso rocks— and as inherited zircon cores rather than as whole crystals. Unrecognized zircon inheritance could lead to spurious evidence for significant Quaternary pre-eruption crystallization. At Coso, inheritance does not lead to spurious intermediate ages, i.e., the Devils Kitchen exhibits a range of Quaternary zircon that significantly pre-date eruption, but no Mesozoic ages have been obtained, whereas the younger Coso rhyolites exhibit little evidence of zircon growth prior to eruption, yet contain abundant Mesozoic xenocrystic zircon.

The differences reported among zircon age populations contained in individual Coso extrusions are distinct (e.g., the range in time by which they pre-date their respective eruptions) and we believe that they have geologic significance. However, the implications inferred here (and elsewhere), given these apparently distinct age "signatures", make it important to stress that most interpretations are limited by sampling size ($\sim$10's of zircon ages). Where sampling is limited, spot selection and analytical changes may lead to non-representative age spectra and therefore the significance placed on discrete subpopulations, e.g., apparent peaks in zircon age probability density function plots should be interpreted with caution. Nevertheless, the abundance of zircon core ages that significantly pre-date eruption of the Devils Kitchen rhyolite is greater than can be explained by analytical uncertainties alone. Likewise, if the younger Coso rhyolites had had a similar duration of crystallization ($\geq$150 ka), despite their smaller sampling size, statistical arguments would suggest that at least three Quaternary ages $\geq$100 ka older than eruption would be expected but this is not observed. The oldest magmatic zircon age in the younger rhyolites is not resolvable from eruption (at the $\sim$15 ka level).

Evidence for rhyolite source components and crustal assimilation

Evidence of inherited zircon, as well as radiogenic isotope compositions, suggests that a crustal source component was important in the generation of at least some of the Coso rhyolites (e.g., Bacon, et al. 1984; Glazner et al. 2007; Miller et al. 1996; Monastero et al. 2005). The positive and fairly homogenous ε_{Nd} values (+1.0 to +2.5 ε-units) of the Pleistocene rhyolites led Miller et al. (1996) to conclude that much of the mass of the rhyolites originates from mantle-derived basalt, either indirectly by partial remelting of underplated mafic intrusions or directly by differentiation of asthenospheric melts. In a written communication J. Miller indicated that the Devils Kitchen is more mantle-like ($\varepsilon_{Nd} \approx +4$ ε-units) than the more voluminous younger Pleistocene lavas ($\approx +2$ ε-units). Notably, Manley and Bacon (2000) have suggested that the Coso magma system is shallowing and possibly growing. The shift to lower $^{143}Nd/^{144}Nd$ can be attributed to greater amounts of crustal incorporation during rhyolite evolution and may reflect this growth (Miller 1999), although significant amounts of upper crustal assimilation would require significant preheating because of the greater energy requirements that are needed to heat up relatively cool shallow crust (Dufek and Bergantz 2005).

Why do the highly evolved, i.e., Sr-poor, Coso rhyolites retain relatively primitive isotopic affinities if they have incorporated significant amounts of Mesozoic basement, as

implied by the zircon age data reported here? Is it possible that the assimilant was gabbroic and that the isotopic compositions used by, e.g., Glazner et al. (2007) are not entirely representative of the subsurface Mesozoic basement in the zone of rhyolite genesis and/or storage? Mafic intrusions may locally contain abundant zircon (e.g., Paces and Miller 1993) and if partially remelted may generate rhyolites (e.g., Garrison et al. 2007). For example, the Sr and Nd isotopic compositions of lower crustal cumulates and restites associated with Sierrian granitoids erupted in Miocene lavas (Ducea and Saleeby 1998) have isotopic signatures that are similar to those reported by Monastero et al. (2005). Thus, they could be candidates for parental sources that produced the rhyolites by a scenario that involved partial melting, followed by extensive feldspar fractionation in order to generate their extreme depletion in Sr, Ba, and Eu concentrations (Bacon et al. 1981). Alternatively the assimilant may have had a relatively low Sr abundance and therefore have had little leverage on the Sr isotope systematics, e.g., it could have been metasediments where the zircons were recycled previously from Mesozoic basement.

Given the more primitive Nd isotopic composition of the Devils Kitchen rhyolite as compared to the isotopic composition of post-230 ka rhyolites, the latter may reflect generation of discrete melts from (1) partial melting of a hybrid of early Pleistocene mafic rocks that were intruded into the Mesozoic granitoids (i.e., a source that was a physical mixture of Sr-rich mafic rocks with a juvenile isotopic composition and Sr-poor zircon bearing granites) or (2) an evolving magma reservoir that includes rapid piecemeal differentiation of mantle-derived mafic magmas that intruded and partially entrained relatively deep granitic country rock just prior to eruption. Both would have been facilitated by underplating of mafic magma, which is consistent with the mafic xenoliths and enclaves found in some Coso rhyolites (Bacon and Metz 1984). The latter might better explain the unexpected "reversed" crystal morphology of the zircon (Mesozoic grains are euhedral whereas the Pleistocene grains tend to be subhedral, see Fig. 3) and the inverted temperature estimates of the ~85 ka rhyolites (Fig. 8, see below), and does not necessitate differential retention of early inherited zircon. In general, either scenario can explain the evolved compositions of the Pleistocene Coso lavas, their more primitive mantle-derived and relatively homogenous isotopic compositions, and evidence for both mafic xenocrysts (hornblende ± pyroxene ± olivine) and old zircon.

Temperature estimates and zircon stability

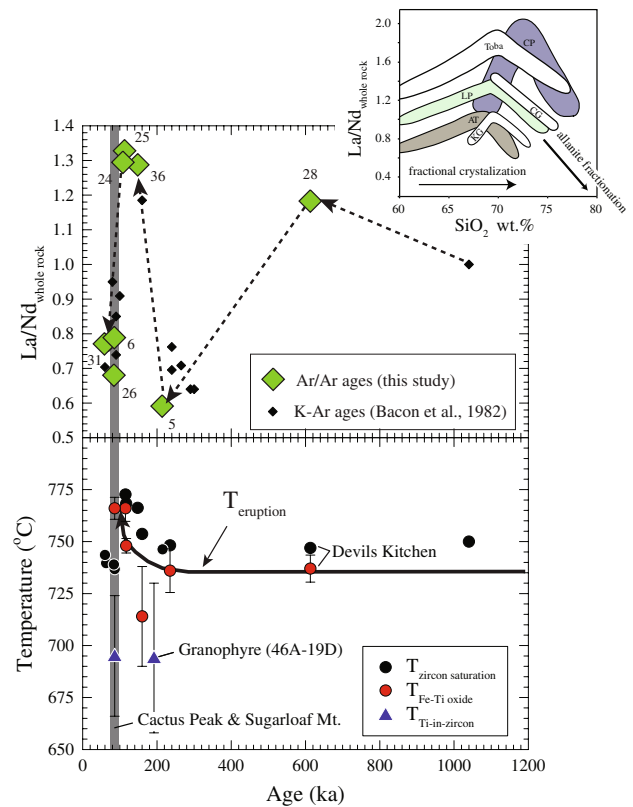The stability of zircon in Coso rhyolites is evaluated by comparing calculated zircon saturation temperatures

Fig. 8 *Upper panel* shows episodic changes in the La/Nd incompatible element ratio of Coso rhyolites through time. *Inset* shows trends of La/Nd in cogenetic suites of silicic magmas related by fractional crystallization of typical mineral assemblages that, at higher degrees of differentiation, include allanite as the dominant light rare-earth element rich accessory phase. The change from increasing to decreasing La/Nd at ~68–72% SiO$_2$ reflects the greater compatibility of La relative to Nd after allanite saturation, with decreasing La/Nd caused by allanite fractionation. *AT* low-intermediate SiO$_2$ Ammonia Tanks Tuff (Mills et al. 1997), *CP* Cordillera Paine granite (Michael 1984), *LP* La Pacana caldera (Lindsay et al. 2001), *CG* Cape Province Granites (Scheepers and Smit 1995), *KG* Kleivan granite series (Petersen 1980), and Toba lavas (Wark et al. 2001). *Zigzag pattern* defined by the Coso rhyolites suggests more complicated open system evolution (see text). *Lower panel* shows Fe–Ti oxide eruption temperatures, calculated zircon saturation temperatures, and Ti-in-zircon temperatures for Coso rhyolites. Symbols defined in figure. *Gray vertical band* links the La/Nd ratios to the temperature estimates for the ~85 ka domes

(Watson and Harrison 1983) to pre-eruption melt temperatures. Zircon saturation temperatures of ~735 to 770°C were determined from the whole rock compositions reported in Bacon et al. (1981). When evaluated chronologically, rather than displaying a secular cooling trend, results for the younger (≤150 ka) Coso rhyolites exhibit a +25°C zircon saturation temperature maximum relative to the older rhyolites (e.g., Devils Kitchen, Fig. 8). By ~90 ka, zircon saturation temperatures had returned to/or dropped slightly below pre-230 ka temperatures.

Pre-eruption temperatures of ~735 to 760°C for individual rhyolites determined by Fe–Ti oxide thermometry

(Manley and Bacon 2000) mimic the trend defined by zircon saturation temperatures. The average temperatures and standard deviations of temperatures computed from multiple oxide pairs for individual rhyolites are plotted in Fig. 8. In most cases the oxide temperatures are equal to or apparently lower than the zircon saturation temperatures. The exceptions are the oxide temperatures of the ∼85 ka Cactus Peak and Sugarloaf Mt. rhyolites, which are ∼20 to 30°C higher than their calculated zircon saturation temperatures (see Fig. 8). Although this temperature inversion is at the upper limit of the uncertainty of the oxide thermometer (±20°C) the systematic increase in both the oxide and zircon saturation temperatures prior to this point lend support to the interpretation that the Coso magmas increased in temperature. Alternatively, the varying temperatures could just indicate discrete melt batches with distinct histories.

Given the calculated zircon saturation and Fe–Ti oxides temperatures, the low Ti-in-zircon temperatures (∼700°C) of the Pleistocene zircon contained in the granophyre and Cactus Peak and Sugarloaf Mt. rhyolites (Fig. 8) are surprising, but consistent with heating after zircon crystallization. In comparison, the average temperature for the Mesozoic zircon is at least 50°C higher than the Pleistocene Ti-in-zircon temperatures. The origin of Mesozoic zircons in Cactus Peak and Sugarloaf Mt. rhyolites is likely linked to their inverted eruption and zircon saturation temperatures (i.e., melt temperatures were probably above the solidus of the surrounding country rocks). As shown by Watson and Harrison (2005) Ti-in-zircon measurements provide maximum zircon crystallization temperature constraints, in part because the a_{TiO2} (=0.42, see earlier Section "Ti-in-zircon thermometry") used to calculate the temperatures are minimum values (i.e., higher a_{TiO2} leads to lower crystallization zircon temperatures). In addition, contamination from cryptic Ti-rich mineral inclusions (e.g., ilmenite) would result in spuriously high Ti-in-zircon temperatures. Accordingly, the Pleistocene zircon crystals likely grew from rhyolite magmas stored as discrete, near-solidus crystal-mushes and/or intrusive bodies that underwent relatively rapid heating just prior to eruption possibly in response to a fresh batch of basaltic magma and/or that the zircon were remobilized just prior to eruption from local, cooler "zero-aged" crystal-mush and/or intrusive bodies.

Coso rhyolite compositional evolution

Like other high-silica rhyolites, those at Coso exhibit little variability among major element abundances (Bacon et al. 1981). Based on their trace element concentrations, e.g., low Sr and Ba and high Rb and Cs (Bacon et al. 1981), differentiation via fractional crystallization was important

in their genesis. However, relative changes in trace elements are difficult to explain by simple, single-reservoir, closed system fractionation. For example, Rb/Sr ratios fluctuating (from ∼20 to ∼260) between successive Coso rhyolite groups imply tapping of discrete magma(s). The ratio La/Nd has been demonstrated to be useful for tracking rhyolite differentiation because of fractionation and differential partitioning related to, light rare earth element-rich accessory minerals (e.g., phases such as allanite, chevkinite, and/ or monazite; Miller and Mittlefehldt (1982) and Vazquez and Reid (2004), see inset in Fig. 8). In allanite-saturated rhyolites, compositional shifts toward higher La/Nd likely equates to input of more mafic magma, although addition of evolved magma where allanite saturation has not occurred could also drive up La/Nd values. Allanite occurs in most Pleistocene rhyolites at Coso (Manley and Bacon 2000), and La/Nd is variable and oscillates through time (Fig. 8). The fluctuating behavior of La/Nd at Coso contrasts with the relatively monotonic increase in La/Nd delineated by rhyolites from the Long Valley magma system that presumably reflects the general shift toward greater input of more primitive magma through time in that system (Simon et al. 2007; see Fig. 9). The fluctuating La/Nd ratios of Coso rhyolites likely suggest that transient and discrete rhyolites characterized the Coso system over time. Magma evolution of a single magma body without rejuvenation would be possible if addition of high La/Nd contaminants to the erupted magma at two alternative times occurred. Contamination by highly evolved basement materials (i.e., low La/Nd ratios) may also have played a role (e.g., there is a significant amount of LREE-depleted peraluminous Mesozoic granite exposed locally, see unpublished basement map of R. Whitmarsh, complied in 1997). Alternatively, a single body of rhyolite could have been periodically recharged and thermally rejuvenated by less evolved melts. If volcanism at Coso was the result of a single evolving magma reservoir, then it is likely that at least two pulses of more primitive rejuvenation occurred (first at ∼625 ka and then at ∼150 ka). The younger rejuvenation pulse at ∼150 ka is the most dramatic because it coincides with a pronounced increase in both zircon saturation and Fe–Ti oxide eruption temperatures. The chemical "recovery" of the differentiating reservoir occurred rapidly, within approximately 40 ka (Fig. 8), but thermal relaxation lagged behind as indicated by the observation that pre-eruption oxide temperatures remained elevated. The presence of abundant euhedral zircon xenocrysts in the ∼85 ka lavas, that contain partially resorbed Pleistocene zircon and allanite grains, is conspicuous because zircon dissolution in hydrous rhyolite at ∼760°C would occur rapidly, i.e., within only hundreds of years depending on number of
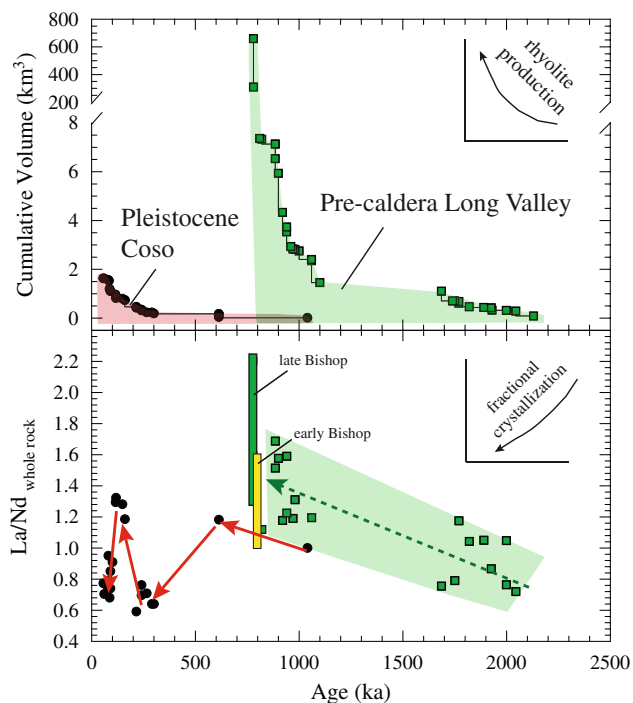
Fig. 9 *Upper panel* shows characteristic increase in rhyolite production (steeper cumulative volume curves) through time at Coso and Long Valley fields. Volume estimates based on Bacon (1982) and Bailey (1989); Metz and Bailey (1993), respectively. *Lower panel* compares La/Nd melt evolution at Coso to Long Valley. Trace element compositions come from Bacon et al. (1981) for Coso rhyolites and Metz and Mahood (1991); Schmitt and Simon (2004) for glasses and Anderson et al. (2000); Peppard et al. (2001); Schmitt and Simon (2004); Wallace et al. (1999) for quartz hosted melt inclusions for Long Valley rhyolites. *Solid arrows* (Coso) and *dashed arrow* (Long Valley) used to clarify temporal trends and should not be mistaken for an implied genetic linkage between sequential eruptions (cf. Simon et al. 2007)

factors such as degree of undersaturation and size (Watson and Harrison 1983). This suggests that the rhyolite body continued to grow by assimilation of country-rock after it experienced recharge and thermal and compositional rejuvenation. It follows, given evidence for zircon inheritance in these rhyolites, that the decreased La/Nd values in the ~85 ka rhyolites might also be the result of crustal assimilation, possibly related to the observed thermal pulse rather than due to very rapid crystallization differentiation. For the ~625 ka positive La/Nd excursion characteristic of Devils Kitchen rhyolite, a concomitant temperature spike is absent. Given clear evidence for mafic injection into the Devils Kitchen magma, this could imply that it erupted from a separate magma body that underwent a distinct compositional (i.e., contaminant) evolution history. This is further evidence that volcanism at Coso tapped at least two (and possibly multiple) distinct magma bodies. Nevertheless, eruption of the Devils

Kitchen magma must have occurred soon enough after injection of the mafic material such that the intruding magma could not have had time to equilibrate chemically with the resident rhyolite. In summary, Coso rhyolites reflect discrete periods of magma genesis dominated by open system behavior whose chemical signatures reflect variable combination of fractional crystallization differentiation, mafic injection and mixing, and at least in some younger rhyolites crustal contamination.

Continuity of the rhyolitic magma reservoir in space and through time

On average it appears that the erupted volumes of rhyolite have increased (Bacon et al. 1981; see Fig. 9), the storage depth of rhyolite has decreased, and rhyolite eruption temperatures have risen (Manley and Bacon 2000; see Fig. 8). Geophysical methods that have claimed to have successfully detect extensive bodies of shallow magma elsewhere (e.g., Eaton et al. 1975) have not demonstrated the existence of shallow magma bodies at Coso, but frequent seismicity (Walter and Weaver 1980), as well as teleseismic P-delay tomography studies (Reasenberg et al. 1980; Wilson et al. 2003), show evidence for a low-velocity body in the middle crust (top of the body at ~5 km below the surface). Given that the volume of intrusive silicic magma at Coso may be as much as 100 times greater than the erupted volume (Bacon et al. 1981) the magma reservoir(s) may have been larger at certain times in the past. Similarities between the extruded domes such as eruption ages, zircon and allanite crystallization ages, and initial Th isotope ratios suggest that at times the erupted part of the Coso rhyolitic magma reservoir was well mixed and integrated (e.g., ~85 ka). These isotopic data lend support to the petrogenetic significance of the geochemical groups of Bacon et al. (1981). The distance between Cactus Peak and Sugarloaf Mountain domes (Fig. 1), implies that at ~85 ka petrologically and geochemically similar magma breached the surface at vents spaced ~5 km apart. This may indicate that the subvolcanic reservoir was of significant lateral extent at the time of eruption. However, given the general alignment of domes extruded at that time, the aspect ratio of this intrusion might be extreme, i.e., a dike that propagated from a reservoir focused at the center of the rhyolite field (Bacon et al. 1980). Regardless, demonstrating the possibility that a substantive reservoir existed at certain times in the past does not necessarily indicate that there was a single magma reservoir evolving through time. The Coso magma system is likely to have waxed and waned over time, as suggested for Long Valley by Reid and Coath (2000), Simon and Reid (2005), and Simon et al. (2007).

The significance of accessory mineral crystallization ages for estimates of magma residence time scales and rhyolite production rates

The age constraints of Coso rhyolites suggest that the record of pre-eruption crystallization contained in individual extrusions can be brief (e.g., post-230 ka rhyolite, this study) or protracted (e.g., Devils Kitchen rhyolite, Miller and Wooden 2004). The record determined here for the post-230 ka rhyolites in which there are only near eruption crystal ages is uncommon among silicic extrusions (cf. TIMS ages reported by Crowley et al. 2007), whereas protracted ages like that of the Devils Kitchen are more common (i.e., among ion probe studies summarized in Simon et al. 2008). Although the volcanic history of Coso is distinct from many long-lived silicic volcanic centers, the diversity of pre-eruption zircon and allanite age spans appears analogous to that reported for individual rhyolites at Long Valley (Heumann et al. 2002; Reid and Coath 2000; Reid et al. 1997; Simon and Reid 2005; Simon et al. 2007).

At issue is how to interpret the evidence for whether silicic magma reservoirs remain thermally viable for protracted amounts of time in the upper crust. The approach taken here that directly measures the difference between crystallization age and eruption age, which is usually interpreted as a minimum storage time for magma in its reservoir (e.g., Davies et al. 1994; Reid et al. 1997; van den Bogaard and Schirnick 1995; Vazquez and Reid 2004), assumes that this duration of crystallization places some measurable estimate on the differentiation time and existence of melt in the shallow crust. It remains unclear as how to best translate this evidence into rhyolite production rates (Charlier et al. 2005; Christensen and DePaolo 1993; Davies et al. 1994; Halliday et al. 1989; Jicha et al. 2005; Knesel et al. 1999; Michaut and Jaupart 2006; Reid and Coath 2000; Simon and Reid 2005; Wolff and Ramos 2003). The existence of a long-recognized relationship between the repose interval between explosive eruptions and their volumes (Smith 1979; Trial and Spera 1990) has led to the long-held view that the duration of silicic magma accumulation is proportional to erupted volume (see inset in Fig. 10). It is probable that the general correlation between repose interval and volume likely represents a Gaussian relationship akin to that observed between earthquake magnitude and frequency (Gutenberg and Richter 1944). This relationship may be useful for understanding magma production rates at the global scale when averaged over significant time periods.

The radioisotopic results from Coso and other rhyolites (see Fig. 10) suggest that at least some voluminous rhyolites can be produced relatively rapidly, and many small-volume rhyolites likely reflect magma storage,
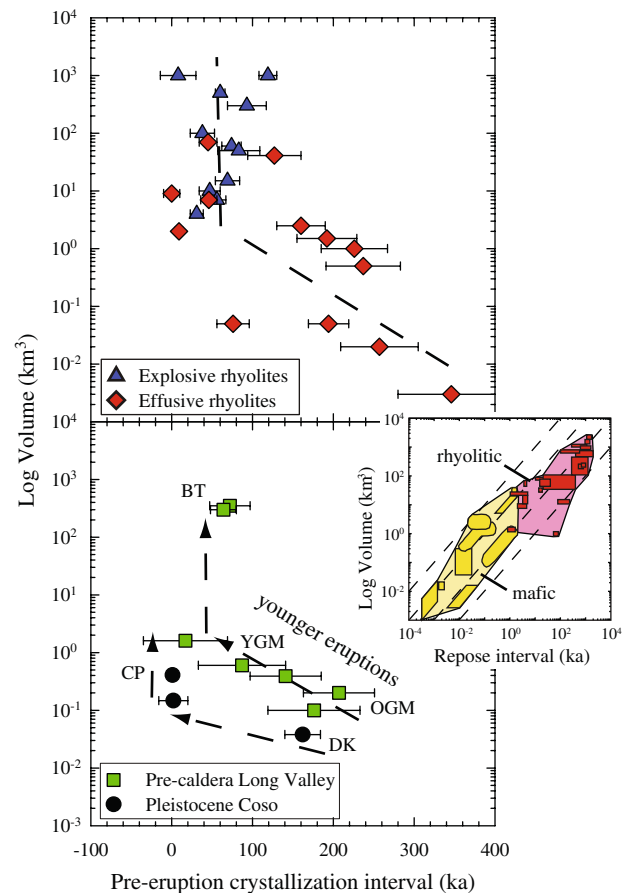

Fig. 10 *Upper panel* shows the pre-eruption time interval for 24 rhyolites based on comparisons between radioisotopic age constraints (e.g., $^{40}Ar/^{39}Ar$ eruption and U–Th–Pb crystallization ages) and magma volume estimated from eruption volume. Data represent a range of volcanic settings from all over the world and come from sources in Simon et al. (2008), as well as from Brown and Smith (2004). Explosive rhyolites (*triangles*) exhibit relatively restricted pre-eruption time intervals (≤120 ka), whereas smaller effusive rhyolites (*diamonds*) trend toward greater time intervals (*dashed line*). *Inset* shows inferred pre-eruption magma residence times and volumes of volcanic rocks. Data sources are in Carrasco-Núñez and Riggs (2008), de Silva and Gosnold (2007), Reid (2003), and Spera and Crisp (1981). *Yellow (light-shaded) fields* for mafic magmas defined in Reid (2003). *Red (dark-shaded) boxes* for evolved magmas show range of uncertainty in volume and repose interval (~inverse eruption frequency). *Lower panel* shows pre-eruption crystallization intervals for select Pleistocene Coso and pre-caldera Long Valley rhyolites, *DK* Devils Kitchen (Miller and Wooden 2004), *CP* Cactus Peak (this study), and *OGM* older Glass Mountain, *YGM* younger Glass Mountain, *BT* Bishop Tuff (Reid and Coath 2000; Simon and Reid 2005; Simon, et al. 2007). The general inverse relationship between size and pre-eruption crystallization interval displayed among different silicic fields (i.e., *upper panel*) exists among individual eruptions at both systems. *Dashed arrows* show that Pleistocene Coso and pre-caldera Long Valley magma systems produced larger eruptions with shorter pre-eruption intervals over time

differentiation, and fractionation in long-lived mushy magma bodies. In addition, Pleistocene Coso and pre-caldera Long Valley rhyolites show similar temporal trends

from: (1) small-volume eruptions that exhibit protracted pre-eruption crystallization intervals to (2) progressively larger-volume rhyolites with dateable crystal evidence preserved only for smaller intervals between early crystallization and eruption. Increased mantle-derived mafic magma production and influx into the silicic magma systems can explain the general characteristics of both systems (e.g., Simon et al. 2007).

Conclusions

Geochemical, geochronological, and isotopic affinities among spatially distinct extrusions at Coso suggest a magmatic evolution characterized by waxing and waning of the system. Distinct zircon and allanite age populations, trace element compositions, and isotopic compositions between sequential eruptions indicate rapid magma differentiation and transient storage of shallow magma bodies over the $\sim$1.1 Ma life time of the system. The unusually high proportion of zircon xenocrysts in the Cactus Peak and Sugarloaf Mountain rhyolites indicate inheritance and assimilation in relatively low temperature magma ($<$800°C). Based on their considerable xenocryst populations, fluctuating incompatible trace element ratios, and Coso's prograde thermal history, it can be seen that some Coso rhyolites were periodically subjected to rejuvenation by intrusion of less evolved magma and characterized by crustal assimilation. More specifically, the succession of Coso rhyolite extrusions either represents: (1) a single long-lived reservoir that incorporated and/ or was rejuvenated by a less evolved component by $\sim$625 ka, then differentiated (by fractional crystallization or contamination by a more evolved component) by $\sim$215 ka, was again rejuvenated by a less evolved component by $\sim$150 ka, and finally incorporated Mesozoic crust as the melts got hotter, consistent with the xenocryst ages showing up in the $\sim$85 ka rhyolites, or (2) the existence of a number of distinct transient magma bodies with relatively distinct proportions of sources that formed and evolved more or less independently.

References

Anderson AT, Davis AM, Lu F (2000) Evolution of Bishop Tuff rhyolitic magma based on melt and magnetite inclusions and zoned phenocrysts. J Petrol 41(3):449–473. doi:10.1093/petrology/41.3.449

Bachmann O, Bergantz GW (2003) Rejuvenation of the Fish Canyon magma body: a window into the evolution of large-volume silicic magma systems. Geology 31(9):789–792. doi:10.1130/G19764.1

Bachmann O, Oberli F, Dungan MA, Meier M, Mundil R, Fischer H (2007) Ar-40/Ar-39 and U–Pb dating of the Fish Canyon magmatic system, San Juan Volcanic field, Colorado: evidence for an extended crystallization history. Chem Geol 236(1–2):134–166. doi:10.1016/j.chemgeo.2006.09.005

Bacon CR (1982) Time-predictable bimodal volcanism in the Coso Range, California. Geology 10(2):65–69

Bacon CR (1985) Implications of silicic vent patterns for the presence of large crustal magma chambers. J Geophys Research B Solid Earth Planets 90(13):1243–1252

Bacon CR, Lowenstern JB (2005) Late Pleistocene granodiorite source for recycled zircon and phenocrysts in rhyodacite lava at Crater Lake, Oregon. Earth Planet Sci Lett 233(3–4):277–293. doi:10.1016/j.epsl.2005.02.012

Bacon CR, Metz J (1984) Magmatic inclusions in rhyolites, contaminated basalts, and compositional zonation beneath the Coso volcanic field, California. Contrib Mineral Petrol 85(4):346–365. doi:10.1007/BF01150292

Bacon CR, Duffield WA, Nakamura K (1980) Distribution of quaternary rhyolite domes of the Coso Range, California—implications for extent of the geothermal anomaly. J Geophys Res 85(5):2425–2433. doi:10.1029/JB085iB05p02425

Bacon CR, Macdonald R, Smith RL, Baedecker PA (1981) Pleistocene high-silica rhyolites of the Coso volcanic field, Inyo County, California. J Geophys Res 86:10223-10241. doi:10.1029/JB086iB11p10223

Bacon CR, Kurasawa H, Delevaux MH, Kistler RW, Doe BR (1984) Lead and strontium isotopic evidence for crustal interaction and compositional zonation in the source regions of Pleistocene basaltic and rhyolitic magmas of the Coso volcanic field, California. Contrib Mineral Petrol 85(4):366–375. doi:10.1007/BF01150293

Bailey RA (1989) Geologic map of the Long Valley Caldera, Mono-Inyo Craters volcanic chain, eastern California. Miscellaneous Investigations Series I-1933. U.S. Geological Survey

Bindeman IN, Valley JW, Wooden JL, Persing HM (2001) Post-caldera volcanism: in situ measurement of U–Pb age and oxygen isotope ratio in Pleistocene zircons from Yellowstone Caldera. Earth Planet Sci Lett 189(3–4):197–206. doi:10.1016/S0012-821X(01)00358-2

Bohrson WA, Reid MR (1998) Genesis of evolved ocean island magmas by deep- and shallow-level basement recycling, Socorro Island, Mexico: constraints from Th and other isotope signatures. J Petrol 39(5):995–1008. doi:10.1093/petrology/39.5.995

Brown SJA, Fletcher IR (1999) SHRIMP U–Pb dating of the preeruption growth history of zircons from the 340 ka Whakamaru Ignimbrite, New Zealand: evidence for >250 k.y. magma residence times. Geology 27(11):1035–1038. doi:10.1130/0091-7613(1999)

Brown SJA, Smith RT (2004) Crystallisation history and crustal inheritance in a large silicic magma system: Pb-206/U-238 ion probe dating of zircons from the 1.2 Ma Ongatiti ignimbrite, Taupo Volcanic Zone. J Volcanol Geotherm Res 135(3):247–257. doi:10.1016/j.jvolgeores.2004.03.004

Carrasco-Núñez G, Riggs NR (2008) Polygenetic nature of a rhyolitic dome and implications for hazard assessment: Cerro Pizarro volcano, Mexico. J Volcanol Geotherm Res 171(3–4):307–315. doi:10.1016/j.jvolgeores.2007.12.002

Charlier BLA, Wilson CJN, Lowenstern JB, Blake S, Van Calsteren PW, Davidson JP (2005) Magma generation at a large, hyperactive silicic volcano (Taupo, New Zealand) revealed by U–Th and U–Pb systematics in zircons. J Petrol 46(1):3–32. doi:10.1093/petrology/egh060

Chen JH, Moore JG (1979) Late Jurassic Independence dike swarm in eastern California. Geology 7(3):129–133

Christensen JN, DePaolo DJ (1993) Time scales of large volume silicic magma systems—Sr isotopic systematics of phenocrysts and glass from the Bishop Tuff, Long Valley, California. Contrib Mineral Petrol 113(1):100–114. doi:10.1007/BF00320834

Claiborne LL, Miller CF, Walker BA, Wooden JL, Mazdab FK, Bea R (2006) Tracking magmatic processes through Zr/Hf ratios in rocks and Hf and Ti zoning in zircons: an example from the Spirit Mountain batholith, Nevada. Mineral Mag 70(5):517–543. doi:10.1180/0026461067050348

Coleman DS, Briggs AS, Glazner AF, Northrup CJ (2003) Timing of plutonism and deformation in the White Mountains of eastern California. Geol Soc Am Bull 115(1):48–57. doi:10.1130/0016- 7606(2003)

Combs J (1980) Heat-flow in the Coso Geothermal Area, Inyo County, California. J Geophys Res 85(5):2411–2424. doi:10.1029/JB085iB05p02411

Crowley JL, Schoene B, Bowring SA (2007) U–Pb dating of zircon in the Bishop Tuff at the millennial scale. Geology 35(12):1123–1126. doi:10.1130/G24017A.1

Dalrymple GB, Grove M, Lovera OM, Harrison TM, Hulen JB, Lanphere MA (1999) Age and thermal history of the Geysers plutonic complex (felsite unit), Geysers geothermal field, California: a Ar-40/Ar-39 and U–Pb study. Earth Planet Sci Lett 173(3):285–298. doi:10.1016/S0012-821X(99)00223-X

Davies GR, Halliday AN, Mahood GA, Hall CM (1994) Isotopic constraints on the production-rates, crystallization histories and residence times of pre-caldera silicic magmas, Long Valley, California. Earth Planet Sci Lett 125(1–4):17–37. doi:10.1016/0012-821X(94)90204-6

de Silva SL, Gosnold WD (2007) Episodic construction of batholiths: insights from the spatiotemporal development of an ignimbrite flare-up. J Volcanol Geotherm Res 167:320–335. doi:10.1016/j.jvolgeores.2007.07.015

Ducea MN, Saleeby JB (1998) The age and origin of a thick mafic–ultramafic keel from beneath the Sierra Nevada batholith. Contrib Mineral Petrol 133(1–2):169–185. doi:10.1007/s004100050445

Dufek J, Bergantz GW (2005) Lower crustal magma genesis and preservation: a stochastic framework for the evaluation of basalt–crust interaction. J Petrol 46(11):2167–2195. doi:10.1093/petrology/egi049

Duffield WA, Bacon CR (1981) Geologic map of the Coso volcanic field and adjacent areas, Inyo County, California. Miscellaneous Investigations I-1200. U.S. Geological Survey

Duffield WA, Bacon CR, Dalrymple GB (1980) Late Cenozoic Volcanism, Geochronology, and Structure of the Coso-Range, Inyo County, California. J Geophys Res 85(5):2381–2404. doi:10.1029/JB085iB05p02381

Eaton GP, Christiansen RL, Iyer HM, Pitt AM, Mabey DR, Blank HR, Zietz I, Gettings ME (1975) Magma beneath Yellowstone National Park. Science 188(4190):787–796. doi:10.1126/science.188.4190.787

Ferry JM, Watson EB (2007) New thermodynamic models and revised calibrations for the Ti-in-zircon and Zr-in-rutile thermometers. Contrib Mineral Petrol 154(4):429–437. doi:10.1007/s00410-007-0201-0

Garrison JM, Reagan MK, Sims KW, Patino LC (2007) (^{226}Ra)/(^{230}Th) disequilibrium and amphibole crystallization in rhyodacite from Ilopango Caldera, El Salvador. EOS Trans AGU 88 (Fall Meet. Suppl., Abstract F591)

Glazner AF, Miller JS, Leeman WP, Johnson BR, Monastero FC (2007) Magmatic evolution of the Coso Geothermal Area, California. Eos Trans AGU 88(52)

Gulson BL, Krogh TE (1973) Old lead components in young Bergell Massif, southeast Swiss Alps. Contrib Mineral Petrol 40(3):239–252. doi:10.1007/BF00373788

Gutenberg B, Richter CF (1944) Frequency of earthquakes in California. Bull Seismol Soc Am 34:185–188

Halliday AN, Mahood GA, Holden P, Metz JM, Dempster TJ, Davidson JP (1989) Evidence for long residence times of rhyolitic magma in the Long Valley magmatic system—the isotopic record in precaldera lavas of Glass Mountain. Earth Planet Sci Lett 94(3–4):274–290. doi:10.1016/0012-821X(89)90146-5

Harrison TM, Schmitt AK (2007) High sensitivity mapping of Ti distributions in Hadean zircons. Earth Planet Sci Lett 261(1–2):9–19. doi:10.1016/j.epsl.2007.05.016

Hayden LA, Watson EB, Wark DA (2007) A thermobarometer for sphene (titanite). Contrib Mineral Petrol 155(4):529–540. doi:10.1007/s00410-007-0256-y

Heumann A, Davies GR, Elliott T (2002) Crystallization history of rhyolites at Long Valley, California, inferred from combined U-series and Rb–Sr isotope systematics. Geochim Cosmochim Acta 66(10):1821–1837. doi:10.1016/S0016-7037(01)00883-3

Jicha BR, Singer BS, Beard BL, Johnson CM (2005) Contrasting timescales of crystallization and magma storage beneath the Aleutian Island arc. Earth Planet Sci Lett 236(1–2):195–210. doi:10.1016/j.epsl.2005.05.002

Johnson CM, Czamanske GK, Lipman PW (1989) Geochemistry of intrusive rocks associated with the Latir volcanic field, New Mexico, and contrasts between evolution of plutonic and volcanic-rocks. Contrib Mineral Petrol 103(1):90–109. doi:10.1007/BF00371367

Knesel KM, Davidson JP, Duffield WA (1999) Evolution of silicic magma through assimilation and subsequent recharge: evidence from Sr isotopes in sanidine phenocrysts, Taylor Creek rhyolite, NM. J Petrol 40(5):773–786. doi:10.1093/petrology/40.5.773

Kovac KM, Moore JN, Rose PE, McCulloch J (2006) Geology of injection well 46A–19RD in the Coso enhanced geothermal systems experiment. Geotherm Resour Counc Trans 30:139–143

Kylander-Clark ARC, Coleman DS, Glazner AF, Bartley JM (2005) Evidence for 65 km of dextral slip across Owens Valley, California, since 83 Ma. Geol Soc Am Bull 117(7–8):962–968. doi:10.1130/B25624.1

Lanphere MA, Baadsgaard H (2001) Precise K–Ar, Ar-40/Ar-39, Rb–Sr and U/Pb mineral ages from the 27.5 Ma Fish Canyon Tuff reference standard. Chem Geol 175(3–4):653–671. doi:10.1016/S0009-2541(00)00291-6

Lanphere MA, Dalrymple GB, Smith RL (1975) K–Ar ages of Pleistocene rhyolitic volcanism in Coso-Range, California. Geology 3(6):339–343

Lindsay JM, Schmitt AK, Trumbull RB, de Silva SL, Siebel W, Emmermann R (2001) Magmatic evolution of the La Pacana caldera system, Central Andes, Chile: compositional variation of two cogenetic, large-volume felsic ignimbrites. J Petrol 42(3):459–486. doi:10.1093/petrology/42.3.459

Manley CR, Bacon CR (2000) Rhyolite thermobarometry and the shallowing of the magma reservoir, Coso volcanic field, California. J Petrol 41(1):149–174. doi:10.1093/petrology/41.1.149

McDowell FW (1983) K–Ar dating—incomplete extraction of radiogenic argon from alkali feldspar. Isot Geosci 1(2):119–126

Metz J, Bailey RA (1993) Geologic map of Glass Mountain. Miscellaneous Investigations Series I-1995. U.S. Geological Survey

Metz JM, Mahood GA (1991) Development of the Long Valley, California, magma chamber recorded in precaldera rhyolite lavas of Glass Mountain. Contrib Mineral Petrol 106(3):379–397. doi:10.1007/BF00324565

Michael PJ (1984) Chemical differentiation of the Cordillera Paine granite (southern Chile) by in situ fractional crystallization. Contrib Mineral Petrol 87(2):179–195. doi:10.1007/BF00376223

Michaut C, Jaupart C (2006) Ultra-rapid formation of large volumes of evolved magma. Earth Planet Sci Lett 250(1–2):38–52. doi:10.1016/j.epsl.2006.07.019

Miller JS (1999) Recent perspectives on the dynamics of small-volume rhyolite magma systems from Coso volcanic field, CA. EOS Trans AGU 80 (Fall Meet. Suppl., Abstract F1178).

Miller CF, Mittlefehldt DW (1982) Depletion of light rare-earth elements in felsic magmas. Geology 10(3):129–133. doi:10.1130/0091-7613(1982)

Miller JS, Wooden JL (2004) Residence, resorption and recycling of zircons in Devils Kitchen rhyolite, Coso volcanic field, California. J Petrol 45(11):2155–2170. doi:10.1093/petrology/egh051

Miller JS, Groves KR, Whitmarsh RS (1996) Sources of the Pleistocene Coso rhyolites: a Nd isotopic perspective. EOS Trans AGU 77 (Fall Meet. Suppl., Abstract F791)

Mills JG, Saltoun BW, Vogel TA (1997) Magma batches in the Timber Mountain magmatic system, southwestern Nevada volcanic field, Nevada, USA. J Volcanol Geotherm Res 78(3–4):185–208. doi:10.1016/S0377-0273(97)00015-2

Min KW, Mundil R, Renne PR, Ludwig KR (2000) A test for systematic errors in Ar-40/Ar-39 geochronology through comparison with U/Pb analysis of a 1.1-Ga rhyolite. Geochim Cosmochim Acta 64(1):73–98

Monastero FC (2002) An overview of industry–military cooperation in the development of power operations at the Coso geothermal field in southern California. Geotherm Resour Counc Bull 31:188–195

Monastero FC, Katzenstein AM, Miller JS, Unruh JR, Adams MC, Richards-Dinger K (2005) The Coso geothermal field: a nascent metamorphic core complex. Geol Soc Am Bull 117(11–12):1534–1553. doi:10.1130/B25600.1

Mordick BE, Glazner AF (2006) Clinopyroxene thermobarometry of basalts from the Coso and Big Pine volcanic fields, California. Contrib Mineral Petrol 152(1):111–124. doi:10.1007/s00410-006-0097-0

Morgan LE, Renne PR, Watkins JM (2007) ^{40}Ar/^{39}Ar dating of volcanic Glass. Eos Trans AGU 88(52). doi:10.1029/2007EO520006 (Fall Meet. Suppl)

Mundil R, Renne PR, Min KK, Ludwig KR (2006) Resolvable miscalibration of the ^{40}Ar/^{39}Ar geochronometer. Eos Trans AGU 87 (Fall Meet. Suppl., Abstract F543)

Nomade S, Renne PR, Vogel N, Deino AL, Sharp WD, Becker TA, Jaouni AR, Mundil R (2005) Alder Creek sanidine (ACs-2): a quaternary Ar-40/Ar-39 dating standard tied to the Cobb Mountain geomagnetic event. Chem Geol 218(3–4):315–338. doi:10.1016/j.chemgeo.2005.01.005

Paces JB, Miller JD (1993) Precise U–Pb ages of Duluth Complex and related mafic intrusions, northeastern Minnesota—geochronological insights to physical, petrogenetic, paleomagnetic, and tectonomagmatic processes associated with the 1.1 Ga midcontinent rift system. J Geophys Res Solid Earth 98(B8):13997–14013. doi:10.1029/93JB01159

Peppard BT, Steele IM, Davis AM, Wallace PJ, Anderson AT (2001) Zoned quartz phenocrysts from the rhyolitic Bishop Tuff. Am Mineral 86(9):1034–1052

Petersen JS (1980) The zoned Kleivan granite—an end member of the anorthosite suite in southwest Norway. Lithos 13(1):79–95. doi:10.1016/0024-4937(80)90065-1

Quidelleur X, Grove M, Lovera OM, Harrison TM, Yin A, Ryerson FJ (1997) Thermal evolution and slip history of the Renbu Zedong Thrust, southeastern Tibet. J Geophys Res Solid Earth 102(B2):2659–2679

Reasenberg P, Ellsworth W, Walter A (1980) Teleseismic evidence for a low-velocity body under the Coso geothermal area. J Geophys Res 85(5):2471–2483. doi:10.1029/JB085iB05p02471

Reid MR (2003) Timescales of magma transfer and storage in the crust. In: Treatise on geochemistry, vol 3. Elsevier, San Diego, pp 167–187

Reid MR, Coath CD (2000) In situ U–Pb ages of zircons from the Bishop Tuff: no evidence for long crystal residence times. Geology 28(5):443–446. doi:10.1130/0091-7613(2000)

Reid MR, Coath CD, Harrison TM, McKeegan KD (1997) Prolonged residence times for the youngest rhyolites associated with Long Valley Caldera: Th-230-U-238 ion microprobe dating of young zircons. Earth Planet Sci Lett 150(1–2):27–39. doi:10.1016/S0012-821X(97)00077-0

Renne PR, Sharp WD, Deino AL, Orsi G, Civetta L (1997) Ar-40/Ar-39 dating into the historical realm: calibration against Pliny the Younger. Science 277(5330):1279–1280. doi:10.1126/science.277.5330.1279

Renne PR, Karner DB, Ludwig KR (1998) Radioisotope dating—absolute ages aren't exactly. Science 282(5395):1840–1841. doi:10.1126/science.282.5395.1840

Renne PR, Farley KA, Becker TA, Sharp WD (2001) Terrestrial cosmogenic argon. Earth Planet Sci Lett 188(3–4):435–440. doi:10.1016/S0012-821X(01)00336-3

Sañudo-Wilhelmy SA, Flegal AR (1994) Temporal variations in lead concentrations and isotopic composition in the southern California Bight. Geochim Cosmochim Acta 58(15):3315–3320. doi:10.1016/0016-7037(94)90060-4

Schärer U (1984) The effect of initial Th-230 disequilibrium on young U–Pb ages—the Makalu case, Himalaya. Earth Planet Sci Lett 67(2):191–204. doi:10.1016/0012-821X(84)90114-6

Scheepers R, Smit CM (1995) Fractionation of the rare-earths in a suite of highly evolved metaluminous granitoids and felsic dykes from the Western Cape Province, South-Africa. J Afr Earth Sci 21(1):71–90. doi:10.1016/0899-5362(95)00090-G

Schmitt AK (2006) Laacher See revisited: high-spatial-resolution zircon dating indicates rapid formation of a zoned magma chamber. Geology 34(7):597–600. doi:10.1130/G22533.1

Schmitt AK, Simon JI (2004) Boron isotopic variations in hydrous rhyolitic melts: a case study from Long Valley, California. Contrib Mineral Petrol 146(5):590–605. doi:10.1007/s00410-003-0514-6

Simon JI, Reid MR (2005) The pace of rhyolite differentiation and storage in an 'archetypical' silicic magma system, Long Valley,

California. Earth Planet Sci Lett 235(1–2):123–140. doi:10.1016/j.epsl.2005.03.013

Simon JI, Reid MR, Young ED (2007) Lead isotopes by LA-MC-ICPMS: tracking the emergence of mantle signatures in an evolving silicic magma system. Geochim Cosmochim Acta 71(8):2014–2035. doi:10.1016/j.gca.2007.01.023

Simon JI, Renne PR, Mundil R (2008) Implications of pre-eruptive magmatic histories of zircons for U–Pb geochronology of silicic extrusions. Earth Planet Sci Lett 266(1–2):182–194. doi:10.1016/j.epsl.2007.11.014

Smith RL (1979) Ash-flow magmatism. In: Geological Society of America, Special Paper 180. Geological Society of America, New York, pp 5–27

Spera FJ, Crisp JA (1981) Eruption volume, periodicity, and caldera area—relationships and inferences on development of compositional zonation in silicic magma chambers. J Volcanol Geotherm Res 11(2–4):169–187. doi:10.1016/0377-0273(81)90021-4

Ton-That T, Singer B, Paterne M (2001) Ar-40/Ar-39 dating of latest Pleistocene (41 ka) marine tephra in the Mediterranean Sea: implications for global climate records. Earth Planet Sci Lett 184(3–4):645–658. doi:10.1016/S0012-821X(00)00358-7

Trial AF, Spera FJ (1990) Mechanisms for the generation of compositional heterogeneities in magma chambers. Geol Soc Am Bull 102(3):353–367. doi:10.1130/0016-7606(1990)

van den Bogaard P, Schirnick C (1995) Ar-40/Ar-39 laser probe ages of Bishop-Tuff quartz phenocrysts substantiate long-lived silicic magma chamber at Long Valley, United States. Geology 23(8):759–762. doi:10.1130/0091-7613(1995)

Vazquez JA, Reid MR (2002) Time scales of magma storage and differentiation of voluminous high-silica rhyolites at Yellowstone caldera, Wyoming. Contrib Mineral Petrol 144(3):274–285

Vazquez JA, Reid MR (2004) Probing the accumulation history of the voluminous Toba magma. Science 305(5686):991–994. doi:10.1126/science.1096994

Wallace PJ, Anderson AT, Davis AM (1999) Gradients in H_2O, CO_2, and exsolved gas in a large-volume silicic magma system: interpreting the record preserved in melt inclusions from the Bishop Tuff. J Geophys Res Solid Earth 104(B9):20097–20122. doi:10.1029/1999JB900207

Walter AW, Weaver CS (1980) Seismicity of the Coso Range, California. J Geophys Res 85(5):2441–2458. doi:10.1029/JB085iB05p02441

Wark DA, Farmer GL, Masturyono MR, McCaffrey R (2001) Interaction of dike-fed, mafic recharge melts with silicic magmas below the Toba caldera complex. In: Eleventh annual V. M. Goldschmidt conference, May 20–24, 2001, Hot Springs, Virginia, abstract no. 3862

Wark DA, Hildreth W, Spear FS, Cherniak DJ, Watson EB (2007) Pre-eruption recharge of the Bishop magma system. Geology 35(3):235–238. doi:10.1130/G23316A.1

Watson EB, Harrison TM (1983) Zircon saturation revisited—temperature and composition effects in a variety of crustal magma types. Earth Planet Sci Lett 64(2):295–304. doi:10.1016/0012-821X(83)90211-X

Watson EB, Harrison TM (2005) Zircon thermometer reveals minimum melting conditions on earliest Earth. Science 308(5723):841–844

Wiedenbeck M, Alle P, Corfu F, Griffin WL, Meier M, Oberli F, Vonquadt A, Roddick JC, Speigel W (1995) Three natural zircon standards for U–Th–Pb, Lu–Hf, trace-element and REE analyses. Geostand Newsl 19(1):1–23. doi:10.1111/j.1751-908X.1995.tb00147.x

Wilson CK, Jones CH, Gilbert HJ (2003) Single-chamber silicic magma system inferred from shear wave discontinuities of the crust and uppermost mantle, Coso geothermal area, California. J Geophys Res Solid Earth 108(B5). doi:10.1029/2002JB001798

Whitmarsh RS (1997) Geologic map of the Cactus Peak 7.5′ quadrangle; Inyo County, California, http://gsamaps.gsajournals.org/maps/10.1130-1998-whitmarsh-coso/cacpea.gif

Wolff JA, Ramos FC (2003) Pb isotope variations among Bandelier Tuff feldspars: no evidence for a long-lived silicic magma chamber. Geology 31(6):533–536. doi:10.1130/0091-7613(2003)031<0533:PIVABT>2.0.CO;2